Heterometallic palladium-iron Metal-Organic Framework as a highly active catalyst for cross-coupling reactions

Eugenia Miguel-Casañ,[†,⊥] Mohanad D. Darawsheh,[†,⊥] Víctor Fariña-Torres,[§] Iñigo J. Vitórica-Yrezábal,[‡] Eduardo Andres-Garcia,[†] Martín Fañanás-Mastral*[,§] and Guillermo Mínguez Espallargas*[,†]

[†] Instituto de Ciencia Molecular (ICMol), Universidad de Valencia, c/ Catedrático José Beltrán, 2, 46980, Paterna, Spain

[§] Centro Singular de Investigación en Química Biolóxica e Materiais Moleculares (CiQUS), Universidade de Santiago de Compostela, 15782, Santiago de Compostela, Spain

[‡] School of Chemistry, University of Manchester, Oxford Road, Manchester M13 9PL, United Kingdom

[⊥] These authors contributed equally to this work

Supporting information

Table of Contents

1. Synthesis 3
2. Crystallographic data 3
3. Chemical characterization 6
3.1 Powder X-ray diffraction (PXRD) 6
3.2 Infrared Spectroscopy (IR) 6
3.3 X-ray photoelectron spectroscopy (XPS) 7
3.5 Inductively Coupled Plasma Mass Spectrometry (ICP-MS) 9
4. Stability tests of MUV-22 9
4.1 Thermal stability 9
4.2 Chemical stability 11
5. Gas adsorption studies 14
5.1 Low-pressure studies 14
5.2 High-pressure studies 14
5.3 Isosteric heat of adsorption 15
5.4 Crystallinity after adsorption 16
6. Catalytic activity 17
6.1 List of starting materials 18
6.2 Optimization studies 18
6.3 Recycling experiments 20
6.4 Leaching test 21
6.5 Compound characterization 22
6.6 Unsuccessful examples 25
6.7 NMR Spectra 26
7. Stability after catalysis 44
7.1. X-ray powder diffraction 44
7.2. X-ray photoelectron spectroscopy 44
7.3. EDAX 46
7.4. SEM 46
7.5. TEM 47
7.6. Gas sorption 47
7.7. Inductively Coupled Plasma Mass Spectrometry (ICP-MS) 47
8. Exchange test with KF 48
9. References 48

1. Synthesis

All reactions were performed under argon atmosphere using oven dried glassware and using standard Schlenk techniques. Solvents were dried using an MBraun SPS 800 system. All chemicals were purchased from Acros Organics Ltd., Aldrich Chemical Co. Ltd., Alfa Aesar, Strem Chemicals Inc., Fluorochem Ltd. or TCI Europe N.V. chemical companies and used without further purification, unless otherwise noted. The palladate linker *trans*-$[Pd_2Cl_2(H_2PDC)_2]$ was synthetized according to a published procedure.[1]

Synthesis of MUV-22. For the solvent-assisted reaction, a solid mixture of $Fe_3O(CH_3COO)_6(ClO_4)\cdot nH_2O$ (14 mg, 0.020 mmol) and *trans*-$[Pd_2Cl_2(H_2PDC)_2]$ (20 mg, 0.039 mmol) was initially briefly grounded. The mixture was placed in a glass tube and acetic acid (20 μL, 0.350 mmol) was added. The tube was flash-freezed with liquid nitrogen and sealed after a cycle of vacuum. Ten of such tubes were heated for 48 h at 170 °C (heating and cooling rate of 6 °C/h). The resulting mixture was washed with ethanol (3 x 25 ml) and then with methanol (6 x 25 ml) for 2 days. Yield: 140 mg (67 %). Phase-purity was confirmed with X-ray powder diffraction, and the heavy atom elements content was checked with EDS and ICP (calc. Pd:Fe:Cl ratio = 1:2:2): EDS: Pd:Fe:Cl ratio =1.0:2.1:2.2; ICP: Pd:Fe ratio of 1.0:1.8. A scale-up procedure (x10) has also proved successful.

2. Crystallographic data

Data collection. X-ray data for compound **MUV-22** were collected with a Rigaku Supernova with microfocus Mo-Kα radiation at 120 K. Data were measured using CrysAlisPro program.

Crystal structure determination and refinement. X-ray data were processed and reduced using CrysAlisPro suite of programmes. Absorption correction was performed using empirical methods (SCALE3 ABSPACK) based upon symmetry-equivalent reflections combined with measurements at different azimuthal angles. The crystal structure was solved and refined against all F^2 values using the SHELX and Olex 2 suite of programmes.[2] Despite of the use of a highly intense X-ray source, crystals of **MUV-22** only diffracted to 1.25 Å of resolution. All atoms were refined anisotropically with the exception of carbon and nitrogen atoms in order to maximize the data/parameter ratio. Chloride atoms were found disordered and were modelled over two positions, where atomic distances were restrained using distance restrains (SHELX; DFIX and SADI). The atomic displacement parameters were restrained using rigid body restrains (SHELX RIGU and SIMU commands). Hydrogen atoms were placed at calculated positions.

Solvent mask protocol in Olex 2 was used to account for the remaining electron density, finding 128 electrons per formula unit, which could correspond to 13 water molecules.

A large number of A and B alerts were caused by the lack of resolution of the data. The R_{int} value is larger than typical values for single crystal X-ray structures.

Table S1. Crystallographic information for the refinement of **MUV-22**.

Identification code	**MUV-22**
Empirical formula	$C_{42}H_{40}Cl_6Fe_6N_6O_{38}Pd_3$
Formula weight	2103.81
Temperature /K	120(2)
Crystal system	cubic
Space group	*Pm*-3*n*
a /Å	22.1165(4)
b /Å	22.1165(4)
c /Å	22.1165(4)
α /°	90
β /°	90
γ /°	90
Volume /Å^3	10818.1(6)
Z	4
ρ_{calc} /g·cm^{-3}	1.292
μ /mm^{-1}	1.477
F(000)	4136.0
Crystal size /mm^3	0.03 × 0.02 × 0.02
Radiation	Mo Kα (λ = 0.71073)
2Θ range for data collection /°	6.642 to 33.03
Index ranges	$-17 \leq h \leq 17$, $-17 \leq k \leq 17$, $-17 \leq l \leq 17$
Reflections collected	54934
Independent reflections	544 [R_{int} = 0.2715, R_{sigma} = 0.0304]
Data/restraints/parameters	544/1/68
Goodness-of-fit on F^2	1.050
Final R indexes [I>=2σ (I)]	R_1 = 0.0491, wR_2 = 0.1274
Final R indexes [all data]	R_1 = 0.0597, wR_2 = 0.1342
Largest diff. peak/hole /e Å^{-3}	0.52/–0.39

CCDC 2131105 contains the supplementary crystallographic data for this paper. These data can be obtained free of charge via www.ccdc.cam.ac.uk/conts/retrieving.html (or from the Cambridge Crystallographic Data Centre, 12 Union Road, Cambridge CB21EZ, UK; fax: (+44)1223-336-033; or deposit@ccdc.cam.ac.uk).

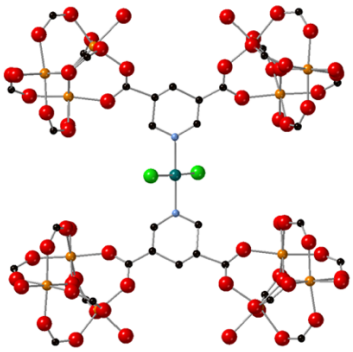

Figure S1. Coordination mode of the metalloligand, in which each of the four carboxylates coordinates to a different SBU.

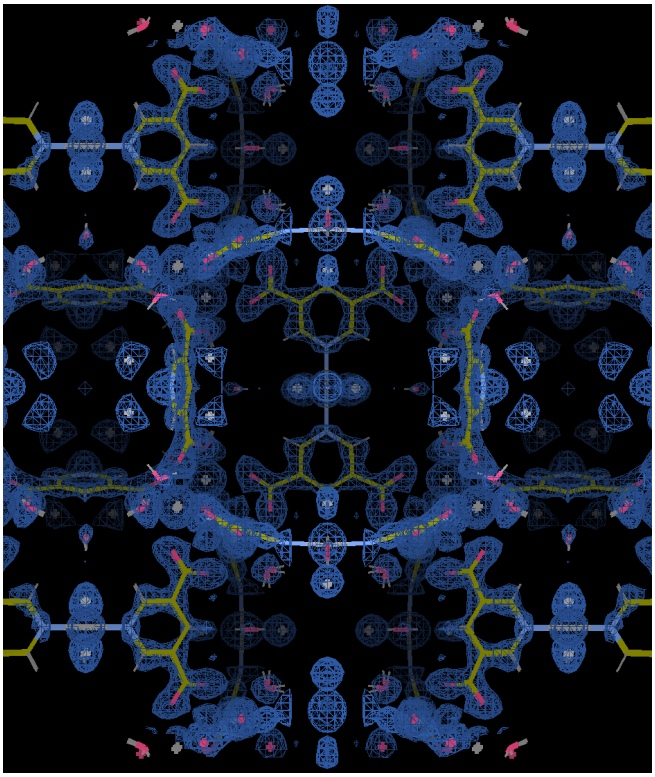

Figure S2. Electron density map (1.2 rdsm) representation with the **MUV-22** structure. Colour code: carbon in yellow, oxygen in pink, palladium, chloride and hydrogen in white.

3. Chemical characterization

3.1 Powder X-ray diffraction (PXRD)

Phase purity of **MUV-22** was established by PXRD. A polycrystalline sample of **MUV-22** was lightly ground in an agate mortar and pestle and filled into a 0.5 mm borosilicate capillary. Data were collected at room temperature in the 2θ range 2–40 ° on an Empyrean PANalytical powder diffractometer, using Cu K_α radiation.

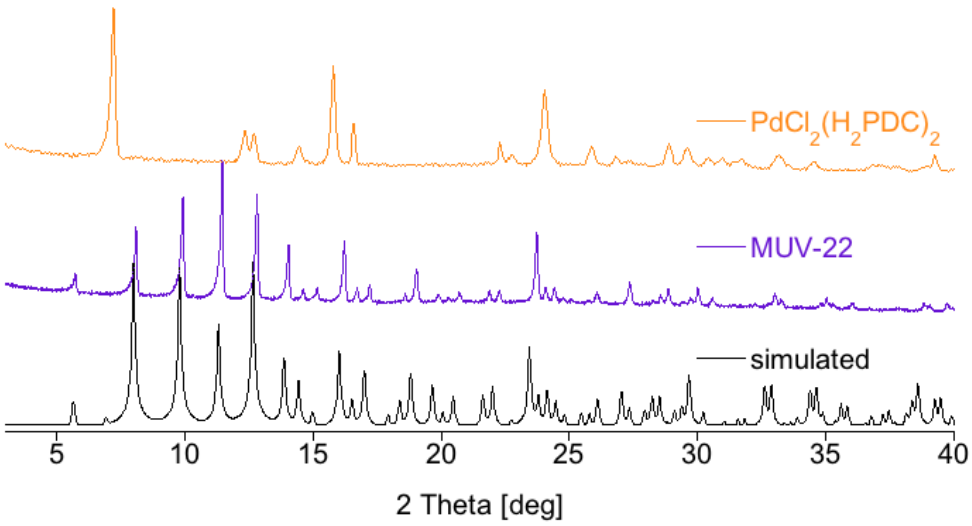

Figure S3. PXRD patterns of **MUV-22** simulated, as-synthetized and $PdCl_2(H_2PDC)_2$.

3.2 Infrared Spectroscopy (IR)

Attenuated total reflectance Fourier-transform infrared (ATR-FTIR) spectra were collected in an Agilent Cary 630 FTIR spectrometer in the 4000–650 cm^{-1} range without using KBr pellets.

The infrared spectrum of **MUV-22** clearly shows the presence of the vibrational bands characteristic of the framework –(C–O–)– groups around 1400 and 1640 cm^{-1} confirming the presence of the dicarboxylate within the solid. On the other hand, the bands at 1718 and 1745 cm^{-1} characteristic of free acid are not observed for washed **MUV-22,** which is in agreement with the absence of uncoordinated ligand within the pores for the solid.[3]

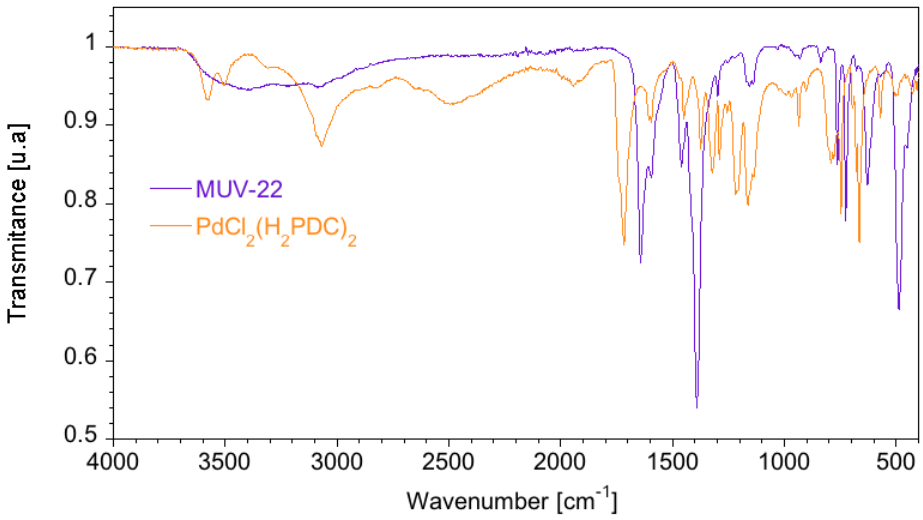

Figure S4. ATR-FTIR spectra of washed **MUV-22** (purple) and $PdCl_2(H_2PDC)_2$ (orange). There is no free metalloligand observed in the MOF.

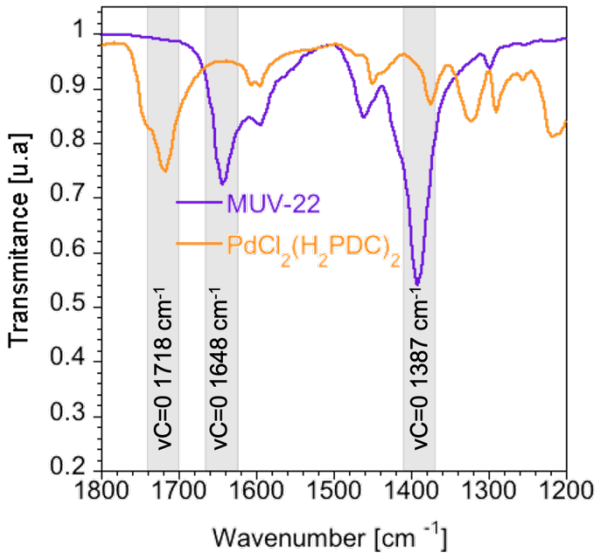

Figure S5. Amplification of the ATR-FTIR spectrum of washed **MUV-22** (purple) and $PdCl_2(H_2PDC)_2$ (orange) in the region 1800–1200 cm^{-1}.

3.3 X-ray photoelectron spectroscopy (XPS)

MUV-22 was prepared by sticking, without sieving, the MOF onto a molybdenum plate with scotch tape film, followed by air drying. Measurements were performed on a K-Alpha™ X-ray Photoelectron Spectrometer (XPS) system using a monochromatic Al-K(alpha) source (1486.6 eV). As an internal reference for the peak positions in the XPS spectra, the C1s peak was set at 284.8 eV.[4]

3.4 Scanning Electron Microscopy (SEM)

Scanning Electron Micrographs images were recorded in a Hitachi S-4800.

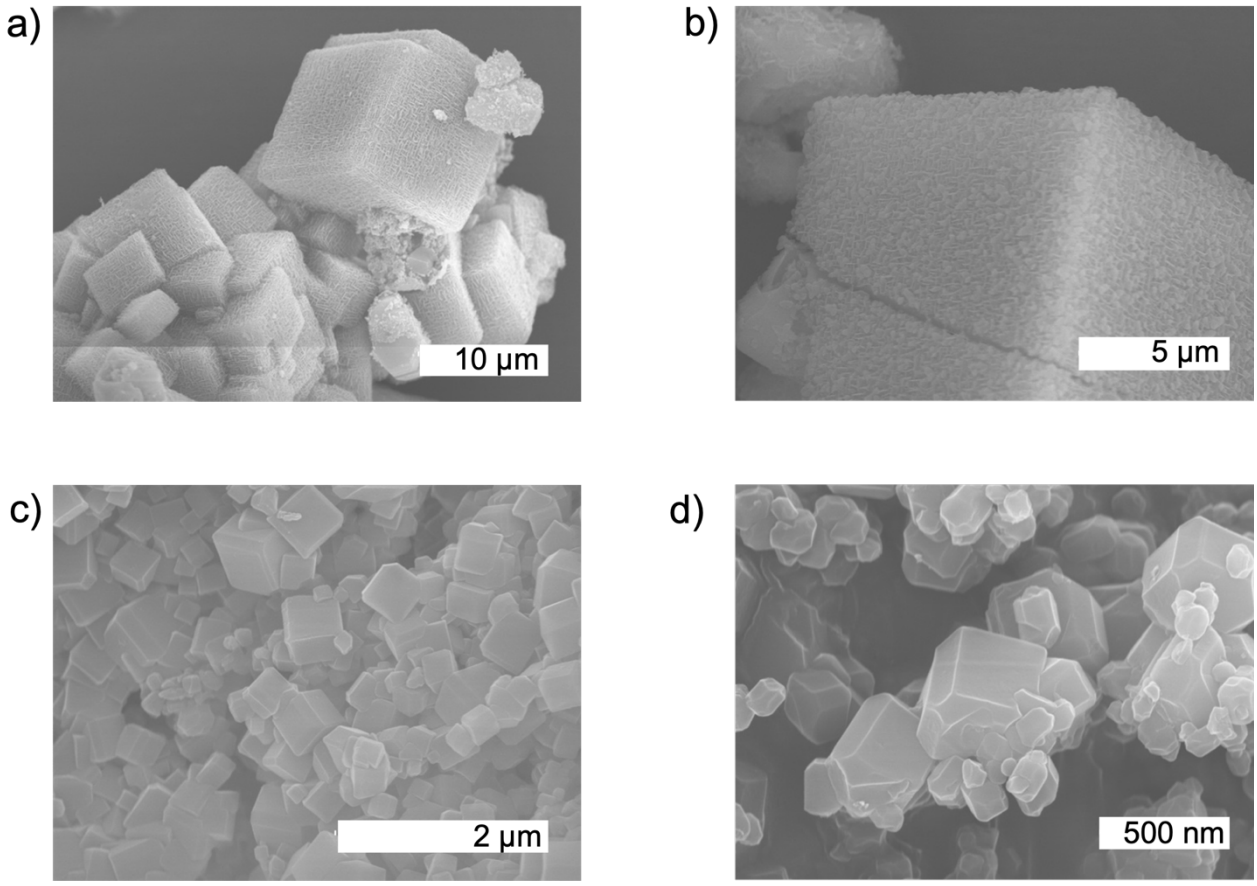

Figure S6. a) Crystals of **MUV-22** with cubic morphology at different scales: a) Scale bar 10 µm; b) Scale bar 5 µm; c) Scale bar 2 µm; d) Scale bar 500 nm.

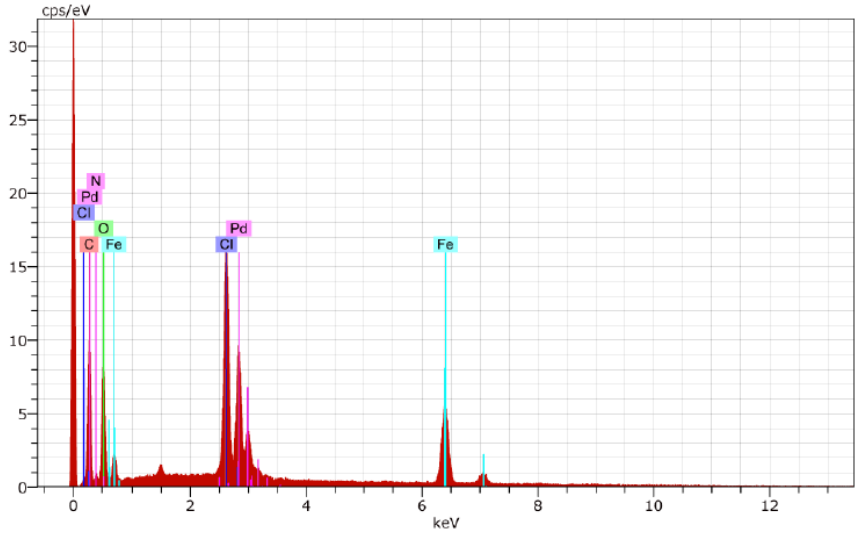

Figure S7. EDS analysis of as-synthesized **MUV-22** showing the presence of the expected elements with a Pd:Fe:Cl ratio = 1.0:2.1:2.2.

3.5 Inductively Coupled Plasma Mass Spectrometry (ICP-MS)

The chemical identity of **MUV-22** was confirmed by inductively coupled plasma mass spectrometry (ICP-MS), using an Agilent model 7900. The amounts of Fe and Pd are 35.6±0.9 (mg/g) and 37.6±0.4 (mg/g), respectively, which indicates the presence of 1.8 Fe per 1 Pd (calc. ratio 2:1).

	mg/g	mmol/g
Fe	35.6±0.9	0.64(2)
Pd	37.6±0.4	0.353(4)

4. Stability tests of MUV-22

4.1 Thermal stability

The thermal stability of **MUV-22** was inspected using Thermogravimetric Analysis (TGA). The initial loss corresponds to the evaporation of solvent molecules. In the range 200–300 °C, a 4 % decrease was observed corresponding to coordinated-water loss (calc. 5 %). Over 310 °C, the MOF decomposes as result of breaking of the metalloligand, as seen in the TGA of the free ligand (Fig S10). Upon heating up to 900 °C, 33 % of residue was remained. The PXRD indicates a mixture of Pd and Fe_2O_3, with a Pd:Fe ratio of 1:1.8 (determined with ICP), which is similar to the ratio determined in the MOF.

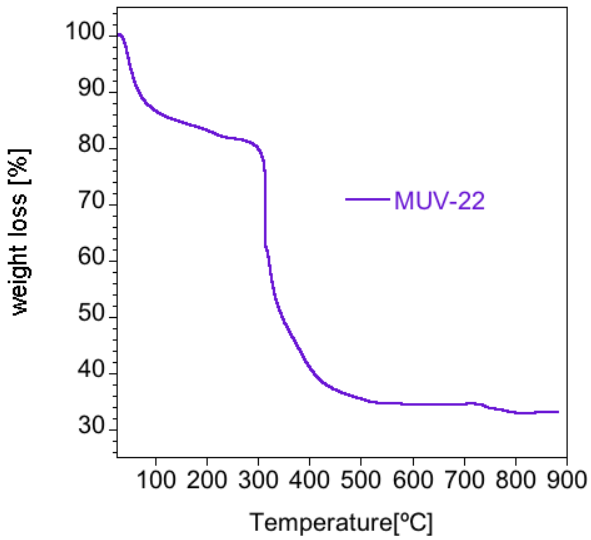

Figure S8. Thermogravimetric analysis (TGA) of **MUV-22** using heating rate of 5 °C/min under air flow.

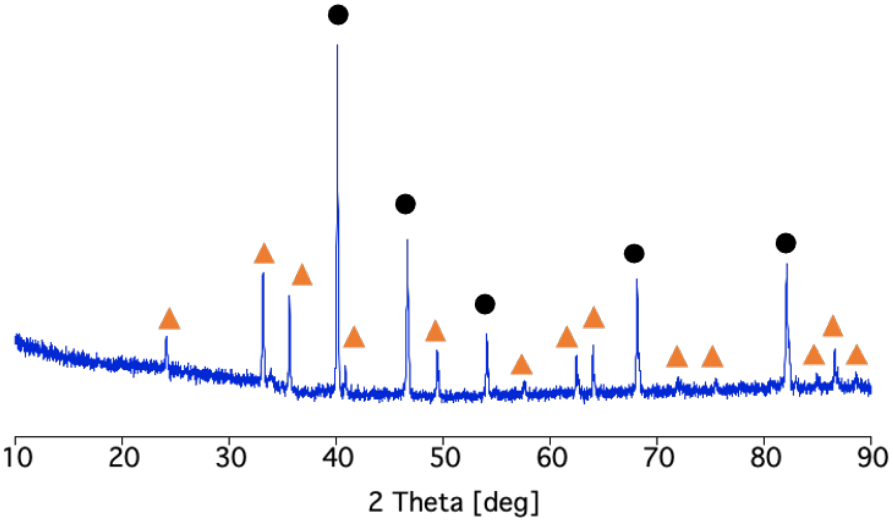

Figure S9. Powder X-ray diffraction pattern of the residue upon heating **MUV-22** up to 900 °C (orange triangles indicate the peaks corresponding to Pd, whereas black circles indicate the peaks corresponding to Fe_2O_3).

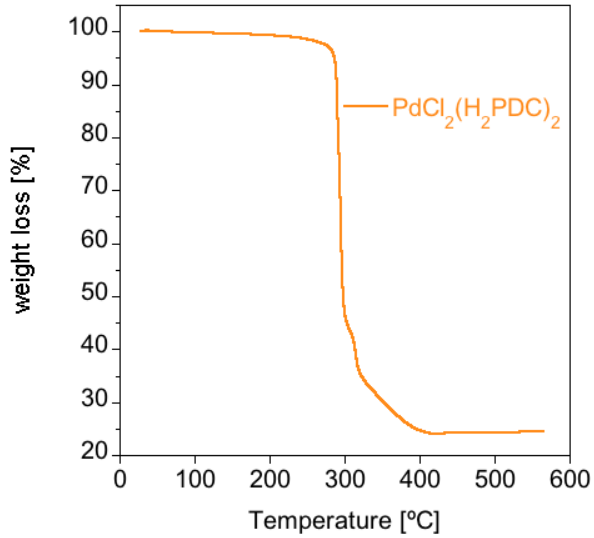

Figure S10. Thermogravimetric analysis (TGA) of the metallo-ligand $PdCl_2(H_2PDC)_2$.

4.2 Chemical stability

The solvent stability of **MUV-22** was evaluated by incubation in different solvents for 24 hours, including aqueous solutions of different pH (pH= 2, 7, and 11). PXRD confirms that the structure of **MUV-22** remains intact after this treatment (see Figure S11 and Figure 3c of the main text).

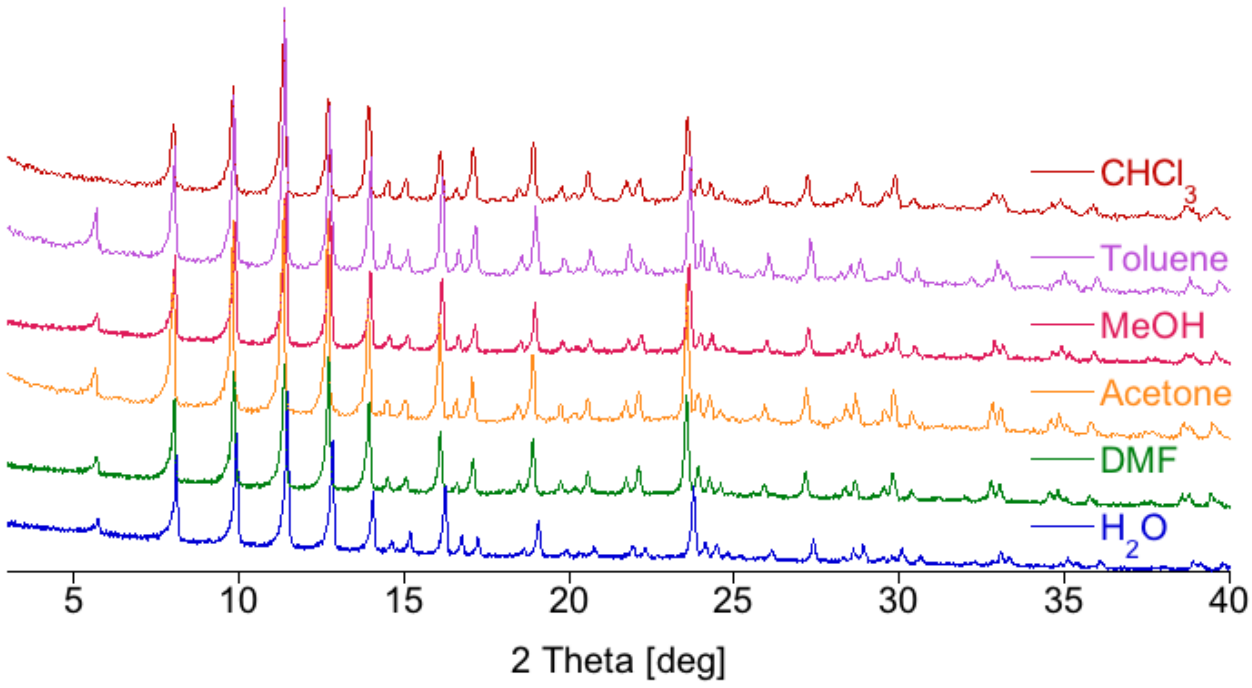

Figure S11. PXRD of **MUV-22** after immersing in different solvents at RT for 24h.

The possible leaching of the MOF was investigated checking the supernatant solution with ^{1}H NMR spectroscopy, to see any presence of organic ligand after 24 h immersion of **MUV-22** in deuterated dioxane, toluene and different deuterated aqueous solutions of pH range between 1-13 (Figure S12).

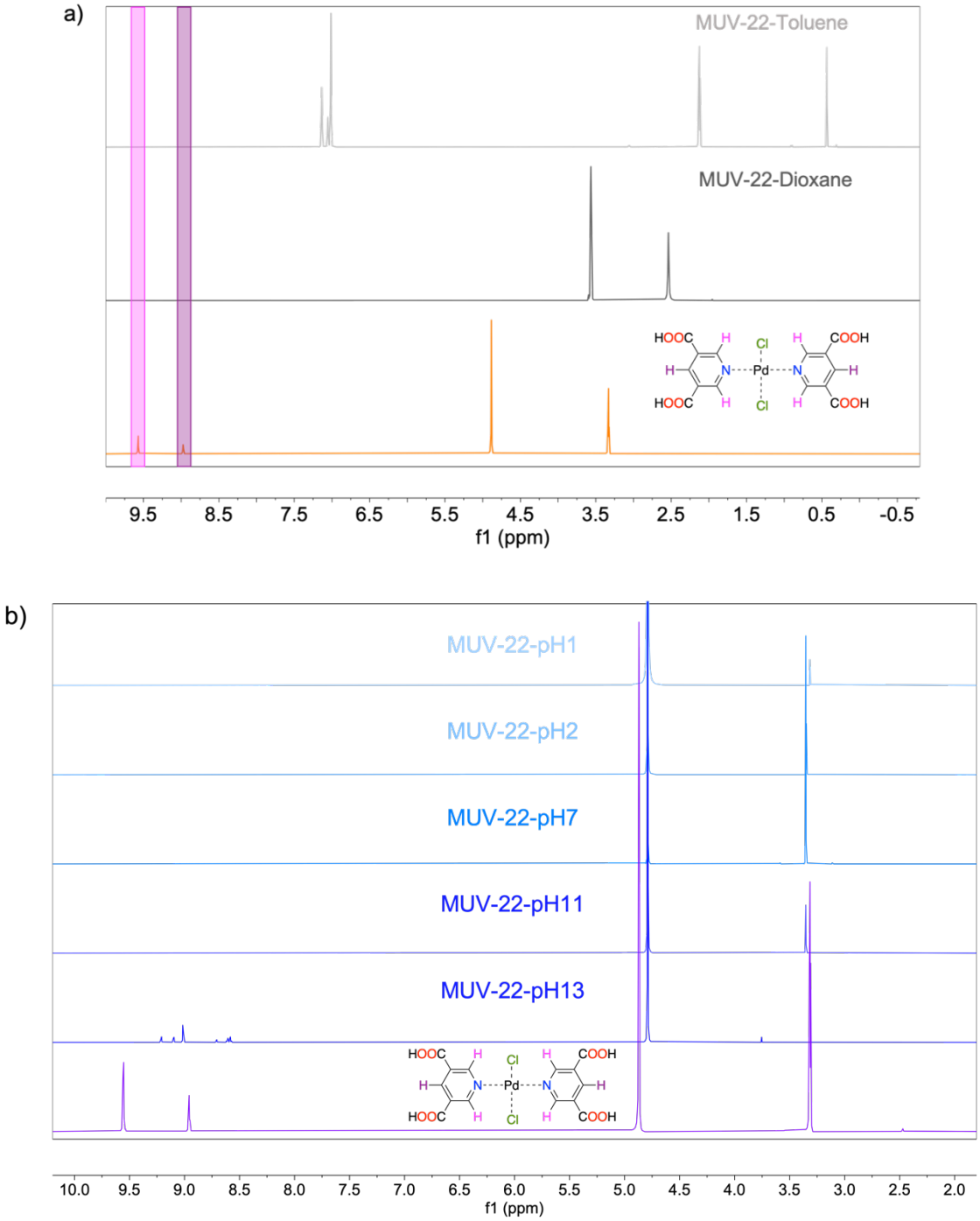

Figure S12. ^{1}H NMR after immersing **MUV-22** in: a) toluene and dioxane (reference spectrum in methanol); and b) different buffered aqueous solutions. No trace of the ligand is observed until pH 13, where some signals in the aromatic region can be observed, likely due to decomposition of the metalolligand.

Finally, **MUV-22** was inspected by thermogravimetric analysis after being incubated in each pH to check the possible formation of defects. Figure S13 shows a similar behavior in all the cases, with the same residual mass.

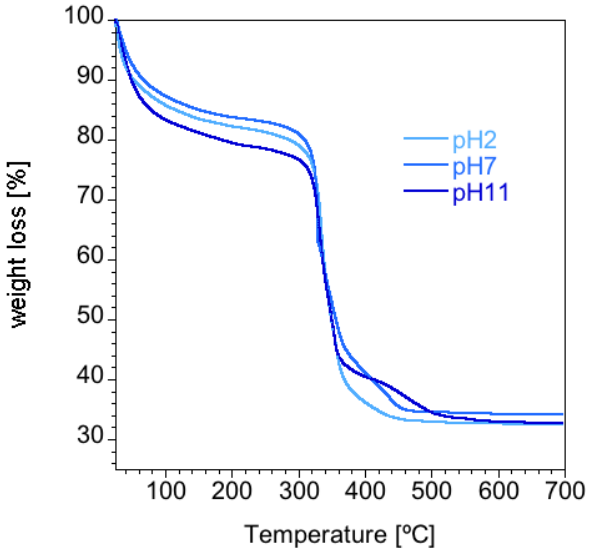

Figure S13. TGA of **MUV-22** after immersing in different buffered aqueous solutions at RT for 24h.

5. Gas adsorption studies

5.1 Low-pressure studies

Low-pressure single-gas nitrogen adsorption isotherms were measured in a Tristar II Plus sorptmeter (Micromeritics), at 77 K. Activation conditions correspond to 393 K, under vacuum, overnight.

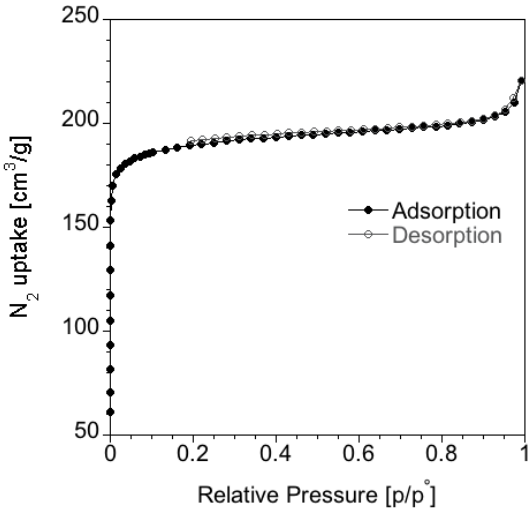

Figure S14. N_2 gas adsorption isotherms of **MUV-22** (solid symbols for adsorption and open ones for desorption).

5.2 High-pressure studies

High-pressure single-gas adsorption isotherms of CO_2, and CH_4 were carried out at different temperatures ranging from 283 to 333 K, in an IGA-100 gravimetric gas sorption analyser (Hiden Isochema) using approximately 40 mg of **MUV-22**. Equilibrium conditions corresponded to 600 s interval, and 0.001 mg·min^{-1} tolerance. Activation was set at 393 K, under vacuum, overnight.

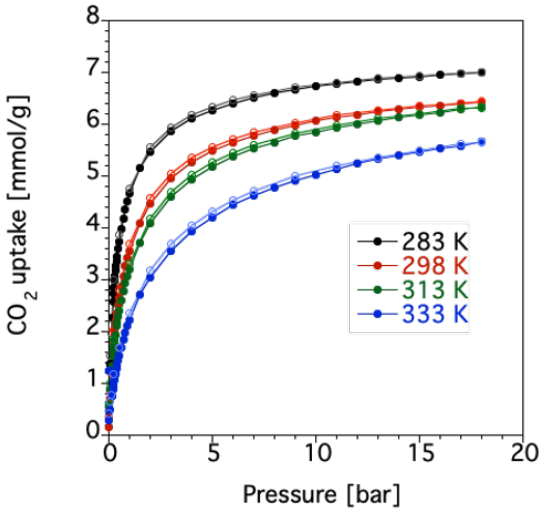

Figure S15. CO_2 gas sorption isotherms of **MUV-22** at different temperatures (solid symbols for adsorption and open ones for desorption).

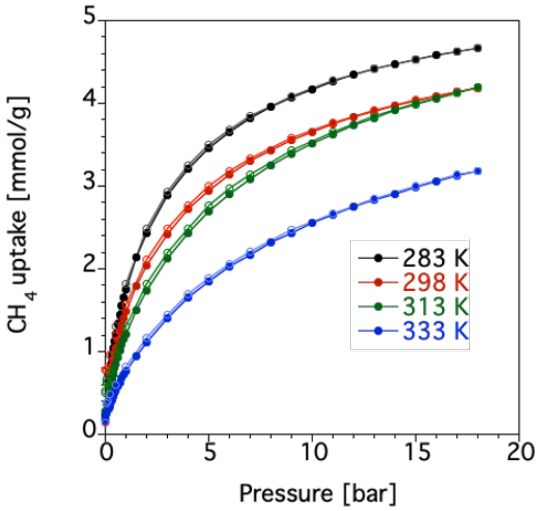

Figure S16. CH_4 gas sorption isotherms of **MUV-22** at different temperatures (solid symbols for adsorption and open ones for desorption).

5.3 Isosteric heat of adsorption

The heat of adsorption was calculated according to the Clausius-Clapeyron equation, and fourth-grade polynomial virial approximation, through the data extracted from the measured gravimetric isotherms, at different temperatures:

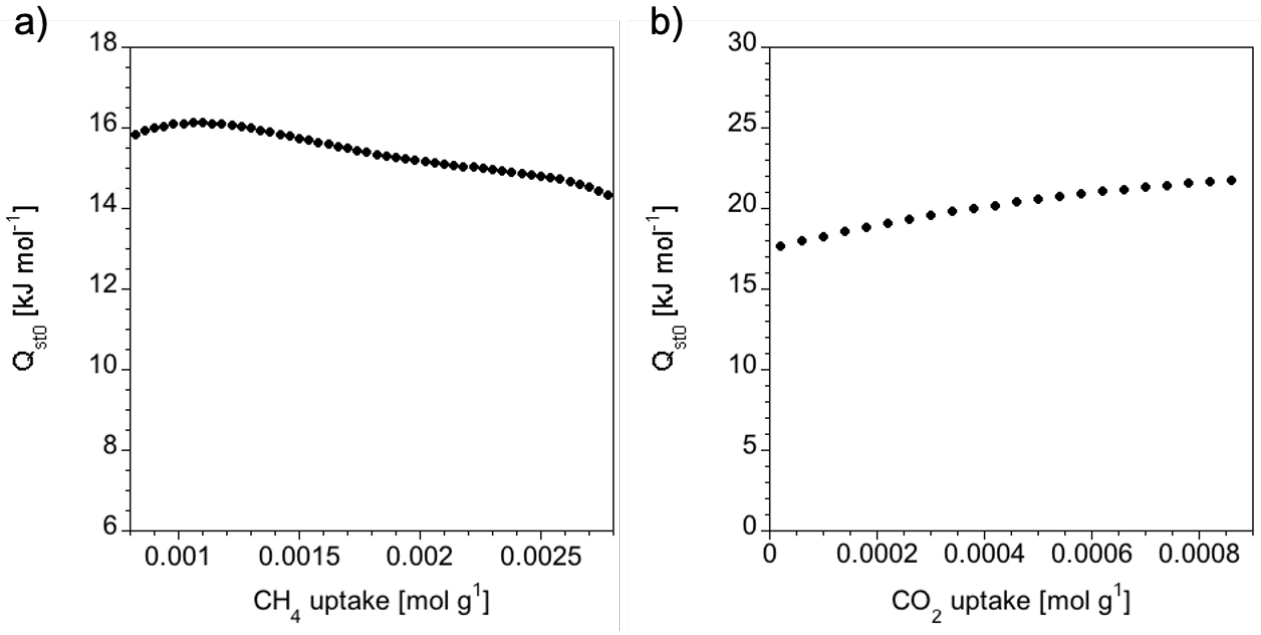

Figure S17. Isosteric heat of adsorption of **MUV-22**: (a) CH_4: q_{st} = 15.1 kJ·mol^{-1}, and (b) CO_2: q_{st} = 22.6 kJ·mol^{-1}.

The isosteric heat of adsorption of the analogours In(III)-MOF is 19.6 kJ·mol^{-1} for CH_4 and 29.8 kJ·mol^{-1} for CO_2.[5] Thus, the values of isosteric heat of adsorption are lower in **MUV-22** for CH_4 and CO_2.

5.4 Crystallinity after adsorption

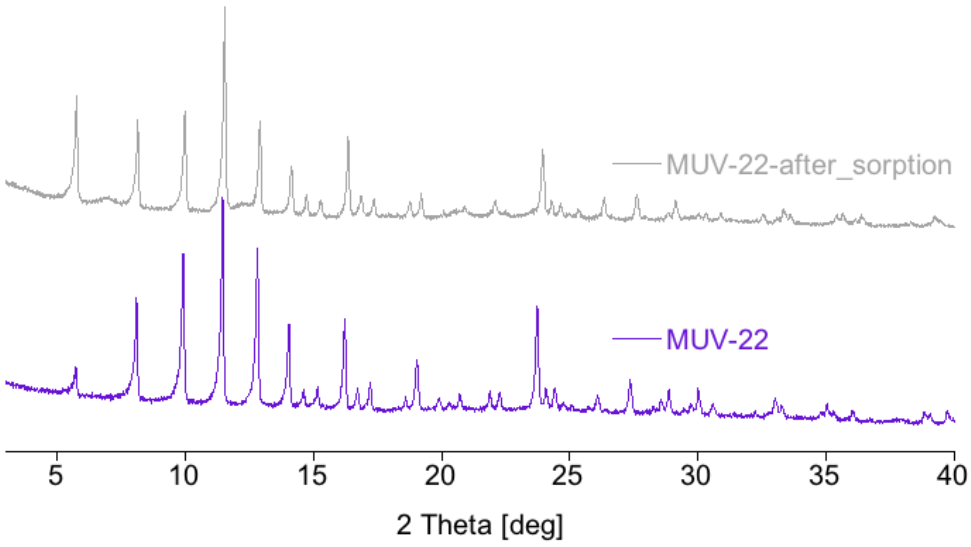

Figure S18. PXRD of **MUV-22** before and after sorption measurements.

6. Catalytic activity

All reactions were performed under argon atmosphere using oven dried glassware and using standard Schlenk techniques. Solvents were dried using an MBraun SPS 800 system. All chemicals were purchased from Acros Organics Ltd., Aldrich Chemical Co. Ltd., Alfa Aesar, Apollo, Strem Chemicals Inc., Fluorochem Ltd. or TCI Europe N.V. chemical companies and used without further purification, unless otherwise noted.

Analytical thin layer chromatography was carried out on silica-coated aluminum plates (silica gel 60 F254 Merck) and components were visualized by UV light and $KMnO_4$ staining. Flash column chromatography was performed on silica gel 60 (Merck, 230-400 mesh).

GC-MS analyses were performed in an Agilent instrument GC-8890 equipped with Chemical Ionization (CI) MS-5977B detector.

High Resolution Mass spectrometry was carried out on a Bruker microTOF spectrometer using APCI.

^{1}H, ^{13}C and ^{19}F NMR spectra were recorded using a Bruker DPX300 (300 MHz), Varian Mercury 300 MHz or Agilent VNMRS-300 MHz NMR spectrometer and Me_4Si as an internal standard. ^{11}B spectra were recorded using a Bruker AVIII 500 MHz. Chemical shift values are reported in ppm with the solvent resonance as the internal standard ($CHCl_3$: δ 7.26 for ^{1}H, δ 77.16 for ^{13}C). Coupling constants (*J*) are given in Hertz (Hz). Multiplicities are reported as follows: s = singlet, d = doublet, t = triplet, q = quartet, p = pentet, m = multiplet or as a combination of them.

High-resolution (MALDI-TOF/TOF) mass spectra were recorded in a 5800 MALDI TOF/TOF (ABSciex) in positive reflector mode.

General procedure for the MUV-22 catalyzed Suzuki-Miyaura allylation

A 5 mL pressure tube equipped with a magnetic stirring bar was charged with **MUV-22** (2.5 mol%), Cs_2CO_3 (0.4 mmol), KF (0.2 mmol). Boronic acid pinacol ester (0.4 mmol) and cinnamyl bromide (0.2 mmol) were dissolved in the corresponding solvent (0.8 mL and 0.2 mL, respectively) and subsequently added to the reaction vessel. The reaction mixture was stirred at the designed temperature for 24 hours. Then, Et_2O (2 mL) was added, and the mixture was decanted. This treatment was repeated 4 times solid. The combined organic layers were filtered through a pad of silica and the solvent was removed under vacuum. Yield was determined by ^{1}H-RMN using dibromomethane as internal standard. The reaction crude was purified by column chromatography with silica gel and isolated yield was obtained.

6.1 List of starting materials

Boronic acid pinacol esters **1a-1h** and allyl bromides **2a** and **2b** were purchased from commercial sources. Boronic acid pinacol ester **1i**[6] and allyl bromides **2c**[7], **2d**[8], **2e**[9], **2f**[7], **2g**[10], **2h**[11], **2i**[12], were prepared according to reported methods.

Boronic acid pinacol esters

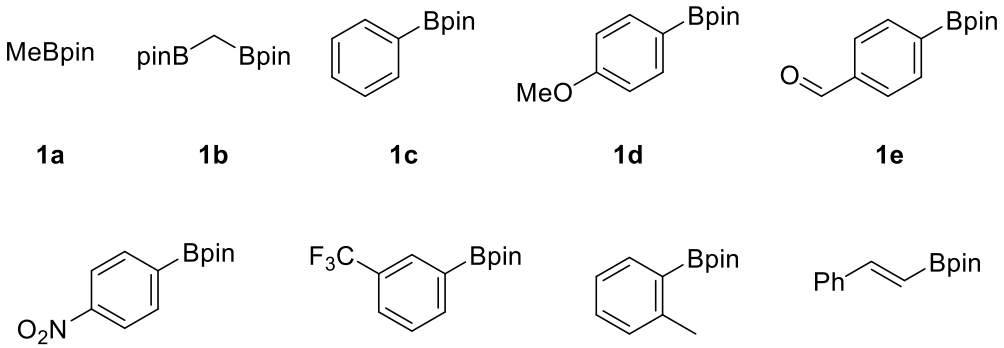

1a **1b** **1c** **1d** **1e**

1f **1g** **1h** **1i**

Allyl bromides

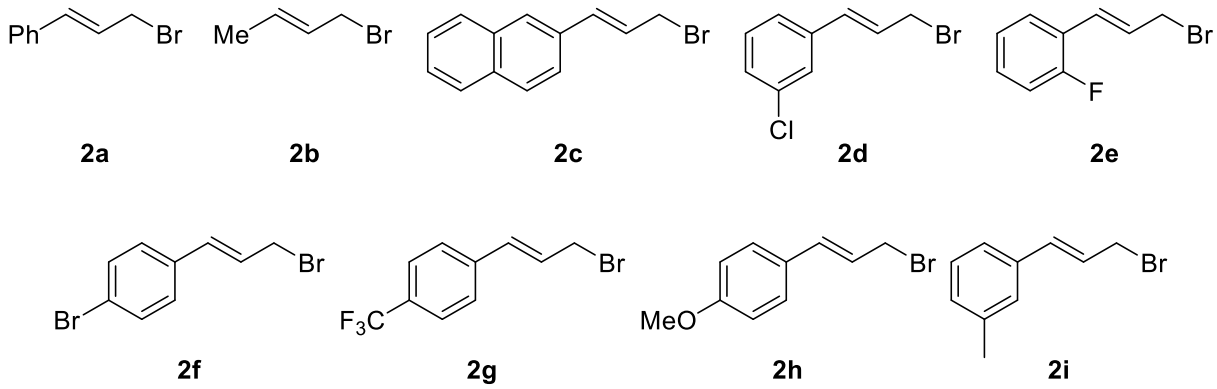

2a **2b** **2c** **2d** **2e**

2f **2g** **2h** **2i**

6.2 Optimization studies

Table S2. Solvent and temperature screening.

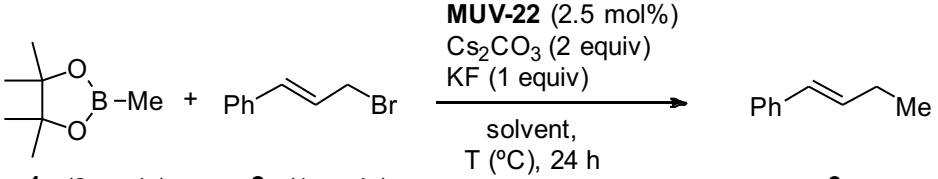

1a (2 equiv) **2a** (1 equiv) **3a**

Entry	Solvent/T	**Conversion** (%)	**3a** (%)	Colour
1	1,4-Dioxane/60 ºC	47	8	Beige
2	1,4-Dioxane/90 ºC	96	23	Beige
3	1,4-Dioxane/120 ºC	100	32	Dark brown
4	Toluene/90 ºC	96	58	Beige
5	Toluene/150 ºC	100	30	Black

Table S3. Screening of different leaving groups.

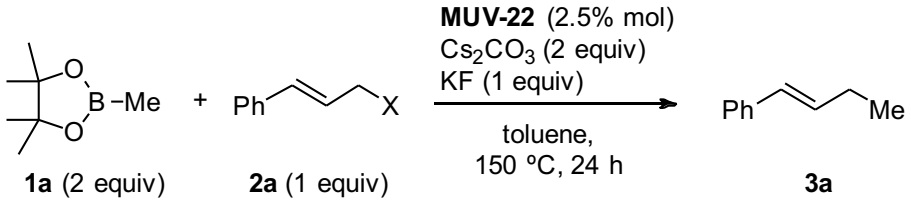

1a (2 equiv) **2a** (1 equiv) **3a**

Entry	X	**Conversion** (%)	**3a** (%)	**Colour**
1	Br	100	35	Black
2	Cl	100	50	Black
3	OBoc	59	7	Black
4	OAc	35	22	Black
5	Cl (at 120 ºC)	87	37	Dark beige
6	Br (at 120 ºC)	100	47	Dark beige

At 150 °C chloride provides a better result than bromide likely due to the decomposition of the bromide at this temperature. However, at 150 °C **MUV-22** gets decomposed (black color) after reaction. At lower temperatures **MUV-22** does not decompose and the chloride gives rise to lower yields than bromide (entries 5 and 6).

Table S4. Screening of additives.

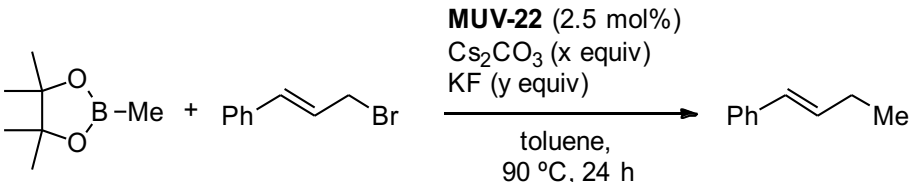

1a (2 equiv) **2a** (1 equiv) **3a**

Entry	**x** equiv	**y** equiv	**Conversion** (%)	**3a** (%)
1	2	1	100	58
2	2	0	100	45
3	0	1	3	-
4	2	0,5	100	40
5	1	1	55	41
6	1	0	49	33
7	3	0	100	44

6.3 Recycling experiments

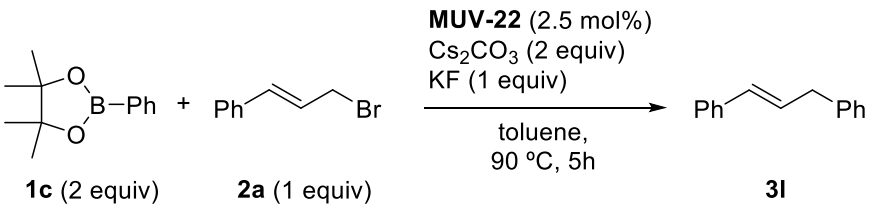

Reaction was run according to the general procedure using cinnamyl bromide (0,4 mmol) and phenylboronic acid pinacol ester (0,8 mmol) as substrates and adding at the start triphenylmethane (0.4 mmol) as internal standard. Aliquots (50 µL) were taken from the reaction every 30 minutes and the yield of the product was determined by ^{1}H-NMR analysis.

After 5 hours the reaction was stopped. The solid was washed Et_2O (5 x 4 mL) and decanted. Finally, it was dried under vacuum. The reaction was set again adding the substrates, additives and internal standard over the recovered solid and it was analyzed as the previous one.

6.4 Leaching test

Reaction was set according to general procedure and adding triphenylmethane (0.2 mmol) as internal standard. After one hour, the reaction mixture was filtered via canula to another sealed tube containing Cs_2CO_3 (0.4 mmol) and an aliquot was taken and analyzed by ^{1}H-NMR. The reaction mixture was allowed to stir under the same conditions and after another hour, the reaction was stopped and it was extracted with Et_2O and filtered through a pad of silica, solvents were removed under vacuum, and it was analyzed by ^{1}H-NMR

a)

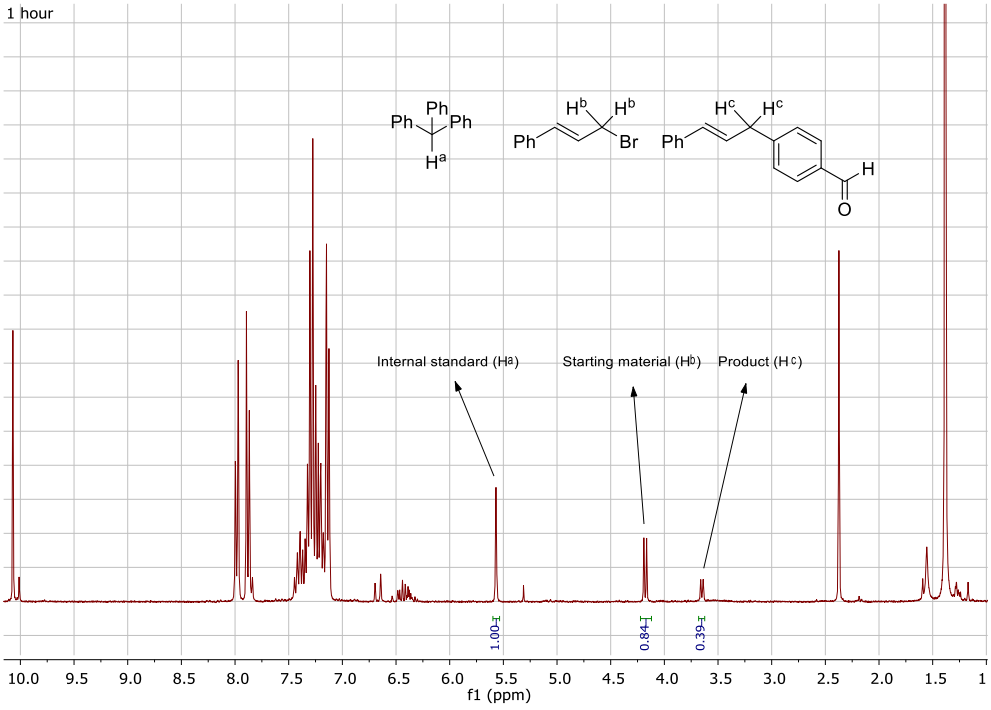

b)

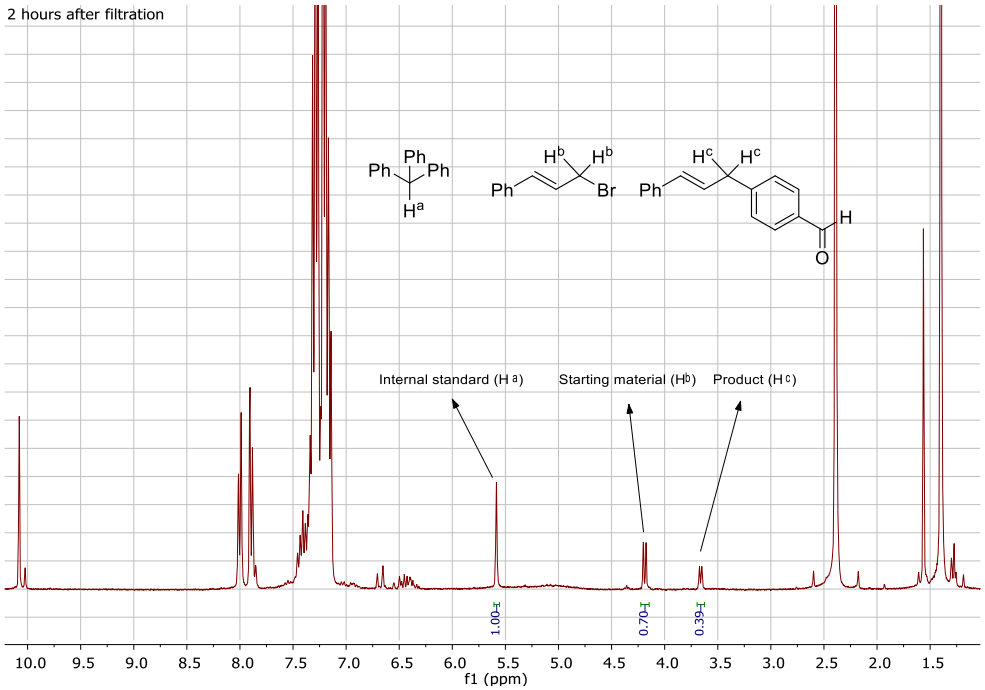

Figure S19. ^{1}H NMR spectra of the reaction after a) 1 hour and b) 2 hours after filtration.

6.5 Compound characterization

(*E*)-But-1-en-1-ylbenzene (3a). Synthesized following the general procedure, obtained as a colorless oil in 58% yield after column chromatography (pentane). **^{1}H NMR** (300 MHz, $CDCl_3$) δ 7.40-7.21 (m, 5H), 6.43 (d, J = 15.8 Hz, 1H), 6.32 (dt, J = 15.8, 6.1 Hz, 1H), 2.28 (m, 2H), 1.15 (t, J = 7.4 Hz, 3H). **^{13}C NMR** (75 MHz, $CDCl_3$) δ 138.1, 132.7, 128.9, 128.6, 126.8, 125.9, 26.0, 13.6. Spectroscopic data are in accordance to reported literature.[13]

(*E*)-2-(But-1-en-1-yl)naphthalene (3b). Synthesized following the general procedure, obtained as a colorless oil in 45% yield after column chromatography (pentane). **^{1}H NMR** (300 MHz, $CDCl_3$) δ 7.78 (m, 3H), 7.68 (m, 1H), 7.58 (m, 1H), 7.43 (m, 2H), 6.55 (d, J = 15.8 Hz, 1H), 6.40 (dt, J = 15.8, 6.2 Hz, 1H), 2.30 (m, 2H), 1.14 (t, J = 7.4 Hz, 3H). **^{13}C NMR** (75 MHz, $CDCl_3$) δ 135.6, 133.9, 133.3, 132.8, 129.1, 128.2, 128.0, 127.8, 126.2, 125.6, 125.4, 123.8, 26.3, 13.8. Spectroscopic data are in accordance to reported literature.[14]

(*E*)-1-(But-1-en-1-yl)-3-chlorobenzene (3c). Synthesized following the general procedure, obtained as a colorless oil in 43% yield after column chromatography (pentane). **^{1}H NMR** (300 MHz, $CDCl_3$) δ 7.33 (s, 1H), 7.22-7.14 (m, 3H), 6.36-6.28 (m, 2H), 2.28-2.19 (m, 2H), 1.09 (t, J = 7.5 Hz, 3H). **^{13}C NMR** (75 MHz, $CDCl_3$) δ 139.6, 134.2, 134.0, 129.4, 127.4, 126.4, 125.6, 123.9, 25.7, 13.2. Spectroscopic data are in accordance to reported literature.[15]

(*E*)-1-(But-1-en-1-yl)-3-methylbenzene (3d). Synthesized following the general procedure, obtained as a colorless oil in 43% yield after column chromatography (pentane). **^{1}H NMR** (300 MHz, $CDCl_3$) δ 7.17 (m, 3H), 7.01 (d, J = 7.0 Hz, 1H), 6.36 (d, J = 16.0 Hz, 1H), 6.25 (dt, J = 15.8, 6.0 Hz, 1H), 2.34 (s, 3H), 2.23 (m, 2H), 1.09 (t, J = 7.4 Hz, 3H). **^{13}C NMR** (75 MHz, $CDCl_3$) δ 138.0, 137.9, 132.5, 128.9, 128.4, 127.5, 126.7, 123.1, 26.1, 21.4, 13.7. Spectroscopic data are in accordance to reported literature.[15]

(*E*)-1-Bromo-4-(but-1-en-1-yl)benzene (3e). Synthesized following the general procedure, obtained as a colorless oil in 45% yield after column chromatography (pentane). **^{1}H NMR** (300 MHz, $CDCl_3$) δ 7.33 (d, J = 8.6 Hz, 2H), 7.13 (d, J = 8.6 Hz, 2H), 6.29 – 6.12 (m, 2H), 2.15 (m, 2H), 1.02 (t, J = 7.5 Hz, 3H). **^{13}C NMR** (75 MHz, $CDCl_3$) δ 136.6, 133.2, 131.2, 128.8, 127.4, 127.2, 120.1, 25.8, 13.2. Spectroscopic data are in accordance to reported literature.[15]

(*E*)-1-(But-1-en-1-yl)-4-(trifluoromethyl)benzene (3f). Synthesized following the general procedure, obtained as a colorless oil in 45% yield after column chromatography (pentane). **^{1}H NMR** (300 MHz, $CDCl_3$) δ 7.53 (d, J = 8.4 Hz, 2H), 7.42 (d, J = 8.0 Hz, 2H), 6.47 – 6.30 (m, 2H), 2.26 (m, 2H), 1.11 (t, J = 7.5 Hz, 3H). **^{13}C NMR** (75 MHz, $CDCl_3$) δ 141.4, 135.5, 127.7, 126.0, 125.4 (q, J = 3.9 Hz), 29.7, 13.4. **^{19}F NMR** (282 MHz, $CDCl_3$) δ -62.4. Spectroscopic data are in accordance to reported literature.[16]

(*E*)-1-(But-1-en-1-yl)-4-methoxybenzene (3g). Synthesized following the general procedure, obtained as a colorless oil in 37% yield after column chromatography (pentane). **^{1}H NMR** (300 MHz, $CDCl_3$) δ 7.27 (d, J = 8.3 Hz, 2H), 6.83 (d, J = 8.7 Hz, 2H), 6.32 (d, J = 15.9 Hz, 1H), 6.12 (dt, J = 15.8, 6.4 Hz, 1H), 3.80 (s, 3H), 2.21 (m, 2H), 1.08 (t, J = 7.4 Hz, 3H). **^{13}C NMR** (75 MHz, $CDCl_3$) δ

158.6, 130.8, 130.5, 128.1, 127.0, 113.9, 55.3, 26.0, 13.8. Spectroscopic data are in accordance to reported literature.[17]

(*E*)-1-Fluoro-2-(3-(3-(trifluoromethyl)phenyl)prop-1-en-1-yl)benzene (3h). Synthesized following the general procedure, obtained as a colorless oil in 45% yield after column chromatography (hexane). **^{1}H NMR** (300 MHz, $CDCl_3$) δ 7.53 – 7.40 (m, 5H), 7.19 (t, J = 6.8 Hz, 1H), 7.14 – 6.97 (m, 2H), 6.66 (d, J = 15.9 Hz, 1H), 6.49 – 6.33 (m, 1H), 3.64 (d, J = 7.0 Hz, 2H). **^{13}C NMR** (75 MHz, $CDCl_3$) δ 159.8 (d, J = 248.7 Hz), 140.6, 131.8, 130.4 (d, J = 4.6 Hz), 130.0 (q, J = 34.1 Hz), 128.7, 128.3 (d, J = 8.4 Hz), 127.5 (q, J = 265.6 Hz), 127.0 (d, J = 3.8 Hz), 125.1 (q, J = 3.9 Hz), 124.6 (d, J = 12.4 Hz), 124.1 (d, J = 3.5 Hz), 123.8 (d, J = 3.6 Hz), 122.9 (q, J = 3.9 Hz), 115.5 (d, J = 22.2 Hz), 39.2.**^{19}F NMR** (282 MHz, $CDCl_3$) δ -62.6, -118.4. **HRMS (APCI)** Calc. for $C_{16}H_{11}F_4$ [M+H$^+$]: 279.0787, found 279.0791.

(*E*)-1-(But-2-en-1-yl)-4-nitrobenzene (3i) + 1-(but-3-en-2-yl)-4-nitrobenzene (3i'). Synthesized following the general procedure, obtained as a pale yellow oil in 69% yield after column chromatography (hexane:DCM 50:50). Obtained as a 2:1 mixture of regioisomers. **^{1}H NMR** (300 MHz, $CDCl_3$) δ 8.17 (m, 2H **3i** + 2H **3i'**), 7.37 (m, 2H **3i** +2H **3i'**), 6.00 (ddd, J = 16.7, 10.4, 6.4 Hz, 1H **3i'**), 5.71 – 5.50 (m, 2H **3i**), 5.17 – 5.07 (m, 2H **3i'**), 3.61 (p, J = 6.9 Hz, 1H **3i'**), 3.44 (m, 2H **3j**), 1.76 – 1.70 (m, 3H **3i**), 1.42 (d, J = 7.0 Hz, 3H **3i'**). **^{13}C NMR** (75 MHz, $CDCl_3$) δ 153.2 (**3i'**), 148.9 (**3i**), 146.5 (**3i'**), 141.4 (**3i'**), 129.2 (**3i**), 129.1 (**3i**), 128.2 (**3i'**), 128.1 (**3i**), 128.1 (**3i**), 127.0 (**3i**), 123.7 (**3i**), 123.7 (**3i'**), 123.6 (**3i**), 114.5 (**3i'**), 43.1 (**3i'**), 38.8 (**3i**), 20.5 (**3i'**), 17.87 (**3i**). **HRMS (APCI)** Calc. for $C_{10}H_{12}NO_2$ [M+H$^+$]: 178.0863, found 178.0863. Spectroscopic data are in accordance to reported literature.[18]

(*E*)-4,4,5,5-Tetramethyl-2-(4-phenylbut-3-en-1-yl)-1,3,2-dioxaborolane (3j). Synthesized following the general procedure, obtained as a colorless oil in 43% yield after column chromatography (hexane:Et_2O 99:1). **^{1}H NMR** (300 MHz, $CDCl_3$) δ 7.39 – 7.17 (m, 5H), 6.41 (d, J = 15.9 Hz, 1H), 6.30 (dt, J = 15.9, 6.1 Hz, 1H), 2.37 (q, J = 7.2 Hz, 2H), 1.27 (s, 12H), 1.01 (t, J = 7.7 Hz, 2H). **^{13}C NMR** (75 MHz, $CDCl_3$) δ 138.0, 132.8, 128.9, 128.4, 126.7, 125.9, 83.1, 27.3, 24.9. **^{11}B NMR** (160 MHz, $CDCl_3$) δ 33.88. Spectroscopic data are in accordance to reported literature.[19]

(*E*)-2-(4-(4-Bromophenyl)but-3-en-1-yl)-4,4,5,5-tetramethyl-1,3,2-dioxaborolane (3k). Synthesized following the general procedure, obtained as a colorless oil in 30% yield after column chromatography (hexane:Et_2O 99:1). **^{1}H NMR** (300 MHz, $CDCl_3$) δ 7.41 (d, J = 7.9 Hz, 2H), 7.20 (d, J = 8.4 Hz, 2H), 6.39 – 6.22 (m, 2H), 2.34 (q, J = 7.5 Hz, 2H), 1.26 (s, 12H), 0.99 (t, J = 7.7 Hz, 2H). **^{13}C NMR** (75 MHz, $CDCl_3$) 137.1, 133.8, 131.6, 127.9, 127.6, 120.4, 83.3, 27.5, 25.0. **^{11}B NMR** (160 MHz, $CDCl_3$) δ 33.88. Spectroscopic data are in accordance to reported literature.[20]

(*E*)-Prop-1-ene-1,3-diyldibenzene (3l). Synthesized following the general procedure, obtained as a colorless oil in 60% yield after column chromatography (hexane). **^{1}H NMR** (300 MHz, $CDCl_3$) δ 7.45 – 7.17 (m, 10H), 6.51 (d, J = 15.9 Hz, 1H), 6.40 (dt, J = 15.8, 6.4 Hz, 1H), 3.59 (d, J = 6.4 Hz, 2H). **^{13}C NMR** (75 MHz, $CDCl_3$) δ 139.9, 137.2, 130.8, 128.9, 128.4, 128.3, 128.2, 128.1, 126.8, 126.1, 125.9, 125.8, 39.1. Spectroscopic data are in accordance to reported literature.[21]

1-Cinnamyl-4-methoxybenzene (3m). Synthesized following the general procedure, obtained as a colorless oil in 54% yield after column chromatography (hexane:Et_2O 99:1). **^{1}H NMR** (300 MHz, $CDCl_3$) δ 7.41 – 7.13 (m, 7H), 6.87 (d, *J* = 8.0 Hz, 2H), 6.45 (d, *J* = 15.9 Hz, 1H), 6.35 (dt, *J* = 16.1, 6.5 Hz, 1H), 3.80 (s, 3H), 3.50 (d, *J* = 6.2 Hz, 2H). **^{13}C NMR** (75 MHz, $CDCl_3$) δ 157.8, 137.3, 131.9, 130.5, 129.4, 129.3, 128.2, 126.8, 125.8, 113.6, 55.0, 38.2. Spectroscopic data are in accordance to reported literature.[22]

4-Cinnamylbenzaldehyde (3n). Synthesized following the general procedure, obtained as a colorless oil in 76% yield after column chromatography (hexane:Et_2O 99:1). **^{1}H NMR** (300 MHz, $CDCl_3$) *δ* 10.01 (s, 1H), 7.85 (d, *J* = 8.2 Hz, 2H), 7.47 – 7.17 (m, 9H), 6.51 (d, *J* = 15.8 Hz, 1H), 6.35 (dt, *J* = 15.8, 6.7 Hz, 1H), 3.65 (d, *J* = 6.7 Hz, 2H).**^{13}C NMR** (75 MHz, $CDCl_3$) *δ* 192.1, 147.7, 137.2, 135.0, 132.3, 130.2, 129.7, 128.7, 127.7, 127.6, 126.3, 39.6. Spectroscopic data are in accordance to reported literature.[23]

1-Cinnamyl-4-nitrobenzene (3o). Synthesized following the general procedure, obtained as a colorless oil in 70% yield after column chromatography (hexane:Et_2O 99:1). **^{1}H NMR** (300 MHz, $CDCl_3$) δ 8.12 – 8.03 (m, 2H), 7.36 – 7.11 (m, 7H), 6.41 (d, *J* = 15.8 Hz, 1H), 6.23 (dt, *J* = 15.8, 6.8 Hz, 1H), 3.57 (d, *J* = 6.7 Hz, 2H). **^{13}C NMR** (75 MHz, $CDCl_3$) δ 148.0, 146.7, 136.9, 132.6, 129.5, 128.7, 127.6, 127.0, 126.2, 123.8, 39.1. Spectroscopic data are in accordance to reported literature.[24]

1-Cinnamyl-3-(trifluoromethyl)benzene (3p). Synthesized following the general procedure, obtained as a colorless oil in 68% yield after column chromatography (hexane). **^{1}H NMR** (300 MHz, $CDCl_3$) δ 7.54 – 7.19 (m, 9H), 6.50 (d, *J* = 15.8 Hz, 1H), 6.34 (dt, *J* = 15.8, 6.7 Hz, 1H), 3.62 (d, *J* = 6.7 Hz, 2H). **^{13}C NMR** (75 MHz, $CDCl_3$) δ 141.2, 137.3, 132.2 (q, *J* = 1,3 Hz), 132.1, 131.0 (q, *J* = 32.1 Hz), 129.0, 128.7, 128.1, 127.5, 126.3, 125.5 (q, *J* = 3.7 Hz), 124.4 (q, *J* = 272.3 Hz), 123.3 (q, *J* = 3.9 Hz), 39.2. Spectroscopic data are in accordance to reported literature.[25]

1-Cinnamyl-2-methylbenzene (3q). Synthesized following the general procedure, obtained as a colorless oil in 72% yield after column chromatography (hexane). **^{1}H NMR** (300 MHz, $CDCl_3$) δ 7.30 – 7.03 (m, 11H), 6.34 – 6.15 (m, 2H), 3.45 (d, *J* = 5.0 Hz, 2H), 2.26 (s, 3H). **^{13}C NMR** (75 MHz, $CDCl_3$) δ 138.4, 137.7, 136.6, 131.0, 130.4, 129.4, 128.7, 128.6, 127.2, 126.5, 126.2, 126.2, 37.0, 19.6. Spectroscopic data are in accordance to reported literature.[26]

(1*E*,4*E*)-1,5-Diphenylpenta-1,4-diene (3r). Synthesized following the general procedure, obtained as a colorless oil in 34% yield after column chromatography (hexane). **^{1}H NMR** (300 MHz, $CDCl_3$) δ 7.44 – 7.21 (m, 11H), 6.52 (d, *J* = 15.9 Hz, 2H), 6.33 (dt, *J* = 15.8, 6.5 Hz, 2H), 3.17 (t, *J* = 6.5 Hz, 2H). **^{13}C NMR** (75 MHz, $CDCl_3$) δ 137.6, 131.2, 128.5, 128.2, 127.1, 126.1, 36.2. Spectroscopic data are in accordance to reported literature.[27]

6.6 Unsuccessful examples

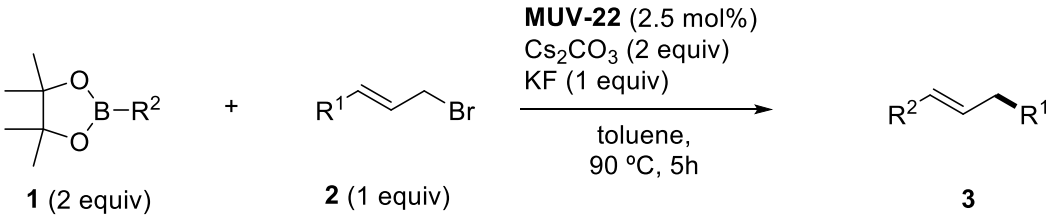

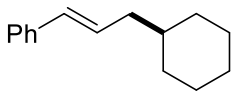

0%

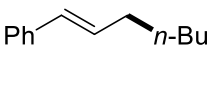

0%

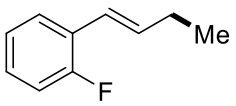

20%

6.7 NMR Spectra

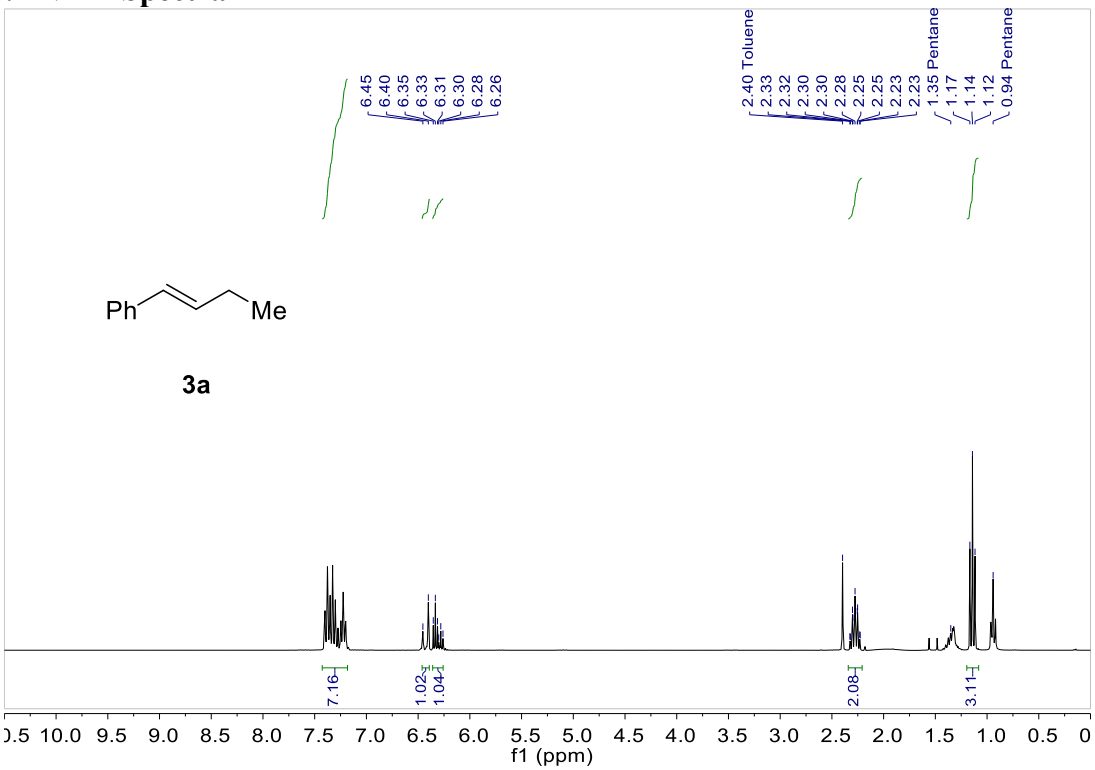

Figure S20. [1]H NMR spectra of product **3a.**

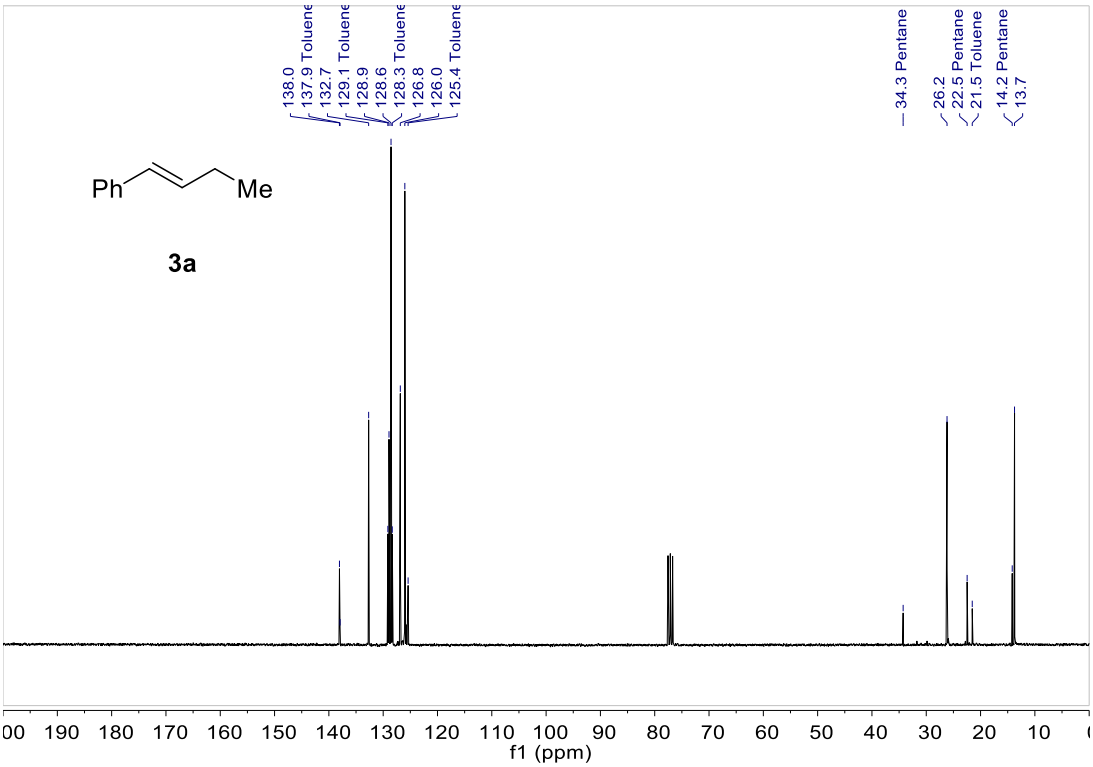

Figure S21. [13]C NMR spectra of product **3a**.

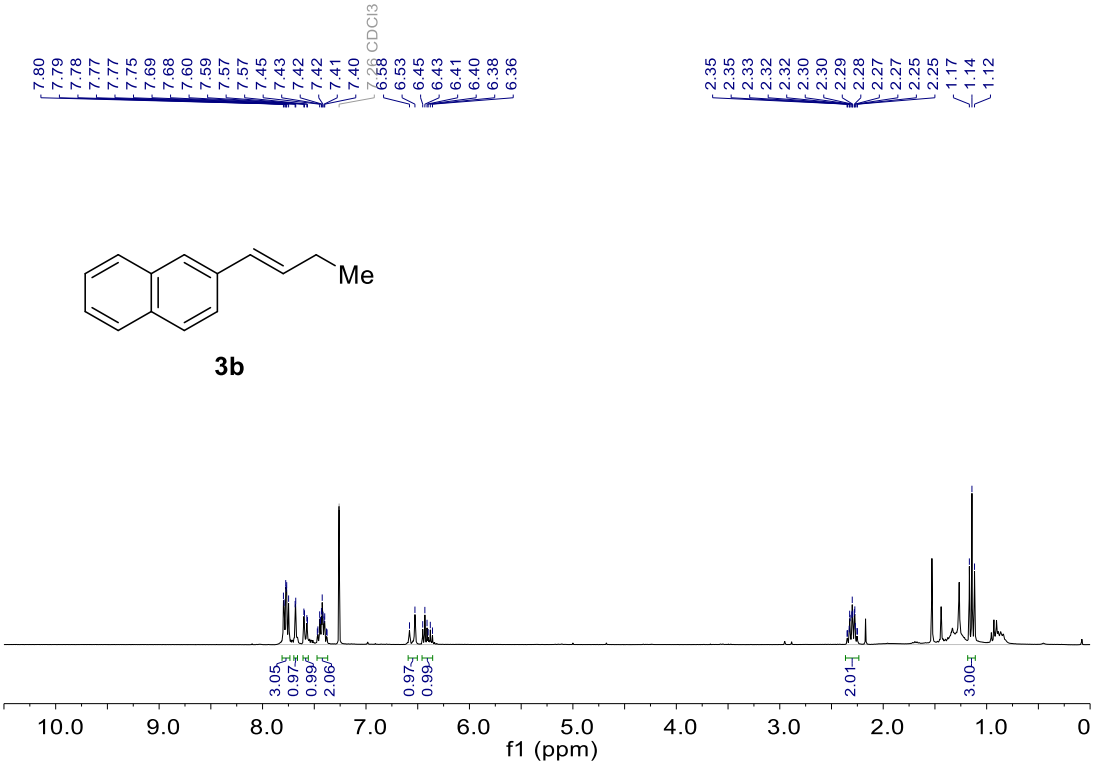

Figure S22. [1]H NMR spectra of product **3b.**

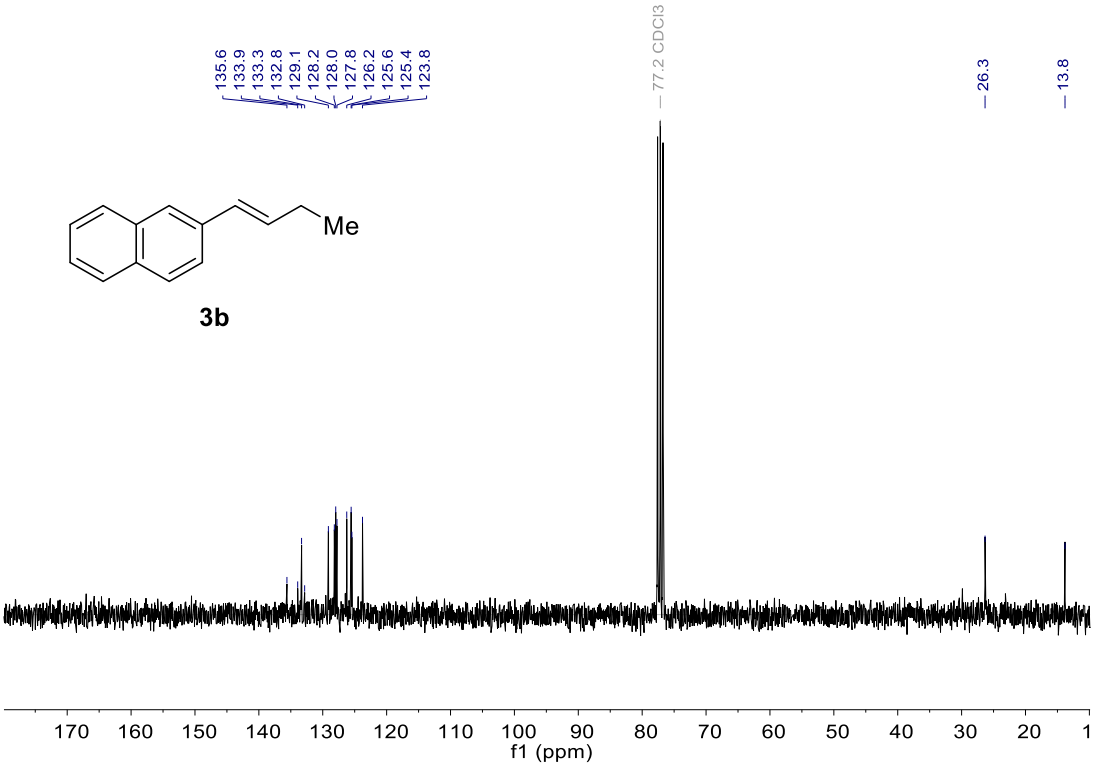

Figure S23. [13]C NMR spectra of product **3b**.

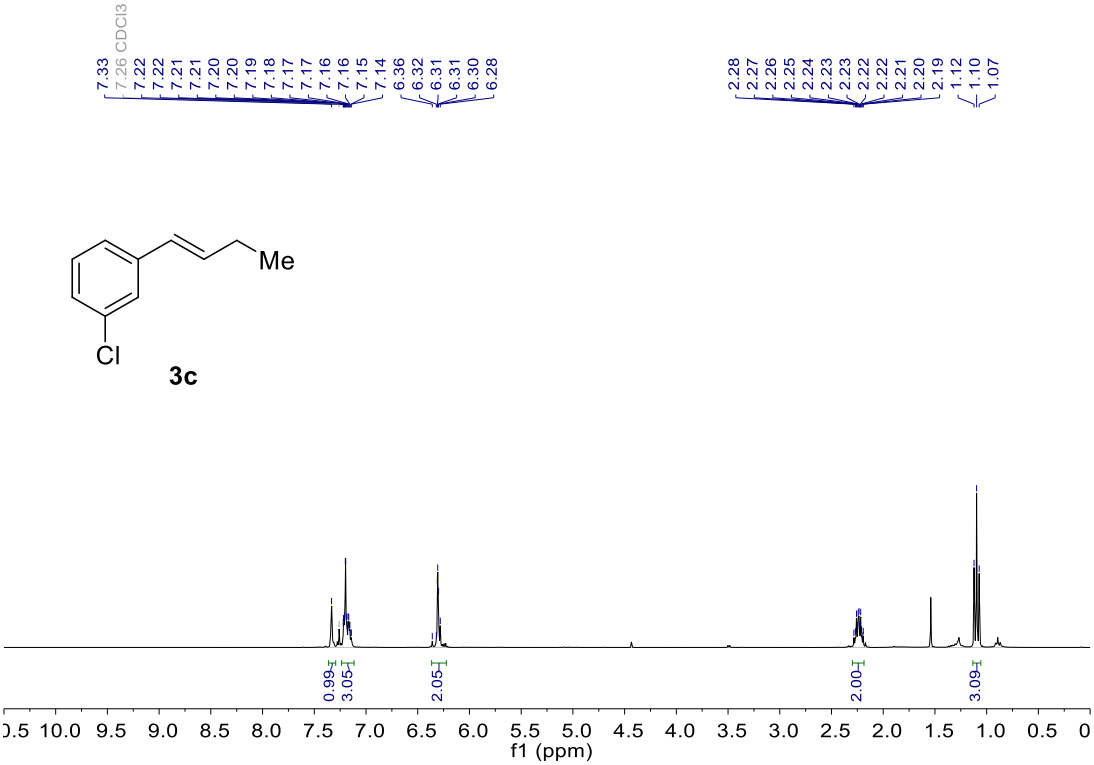

Figure S24. [1]H NMR spectra of product **3c.**

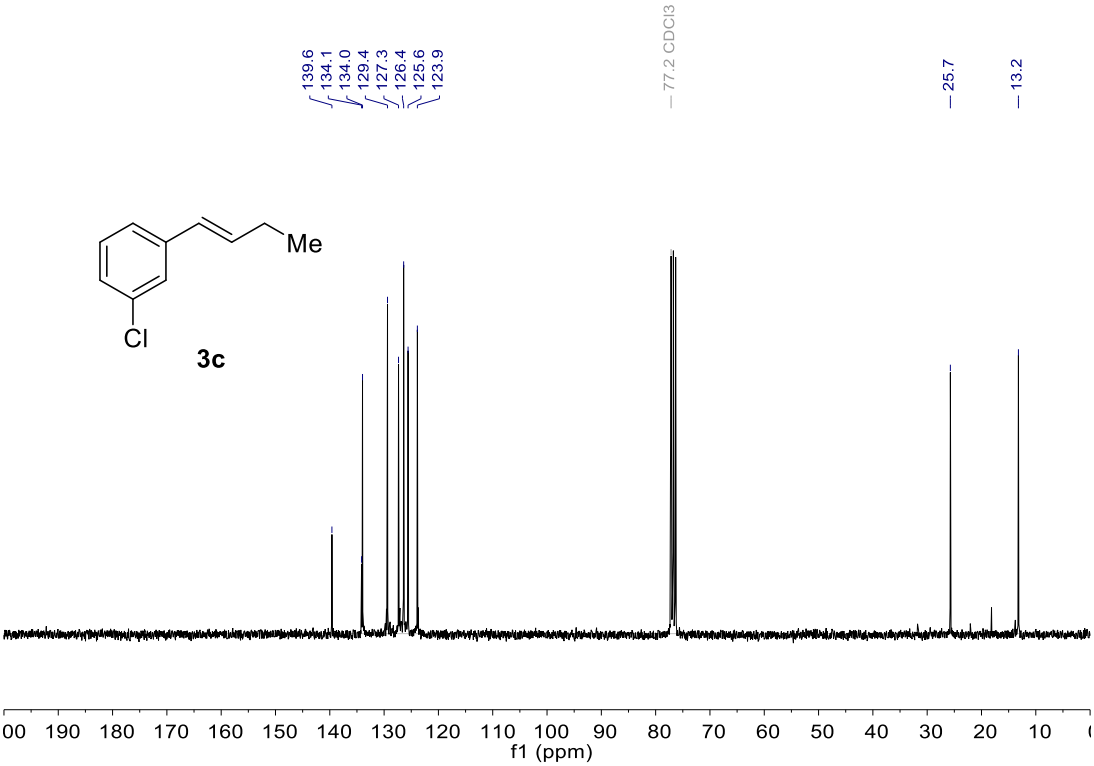

Figure S25. [13]C NMR spectra of product **3c**.

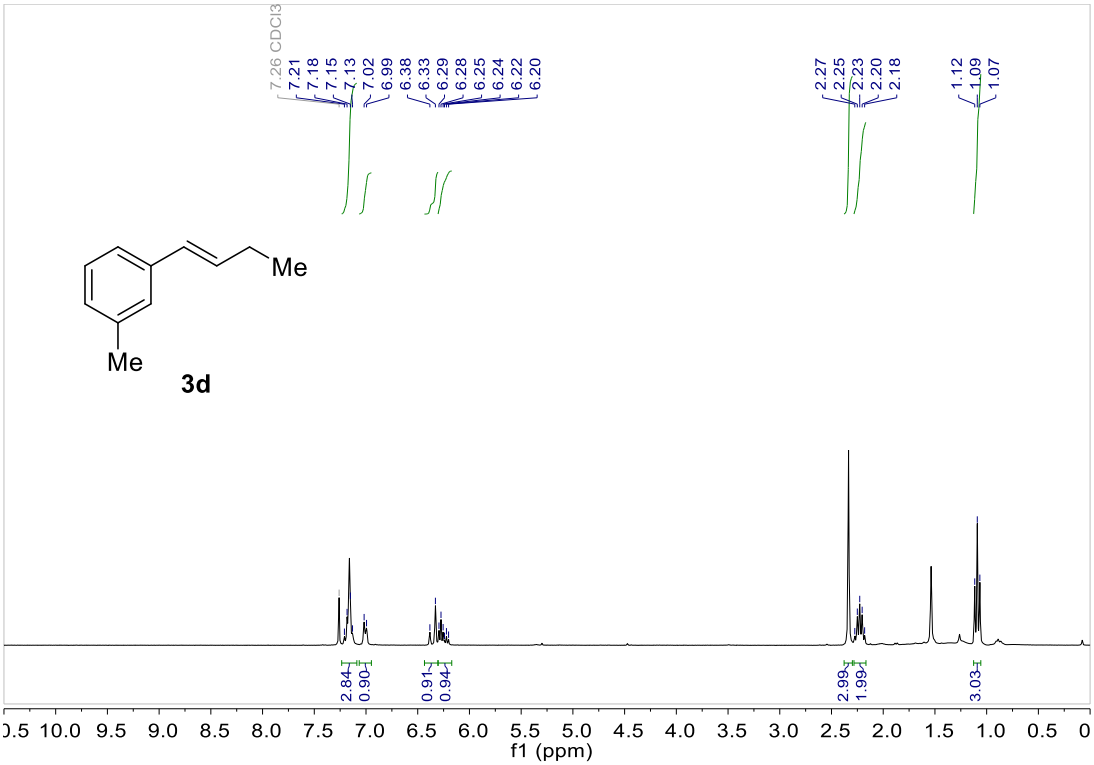

Figure S26. [1]H NMR spectra of product **3d.**

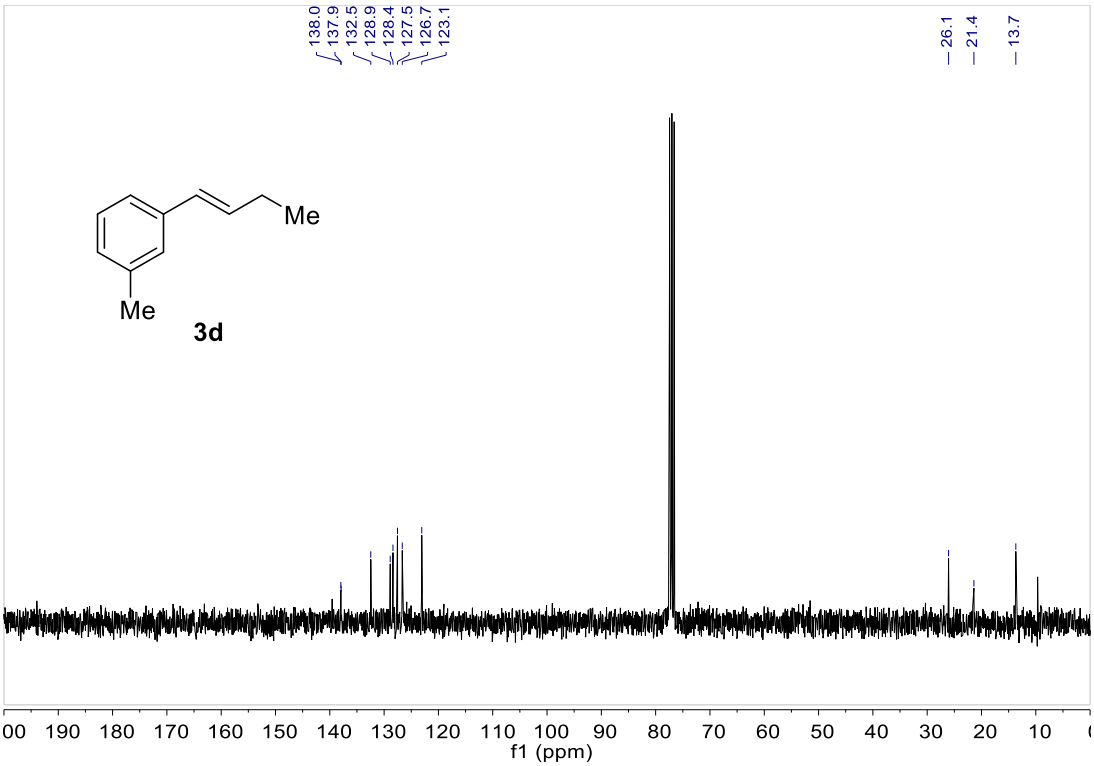

Figure S27. [13]C NMR spectra of product **3d.**

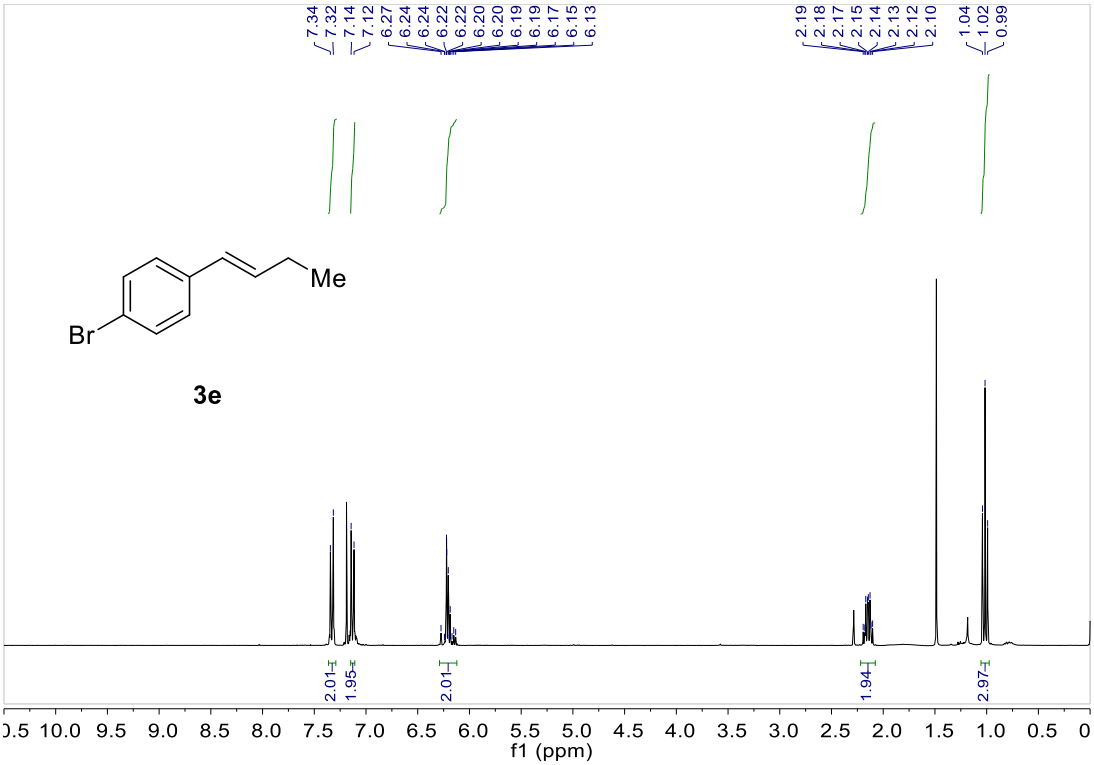

Figure S28. [1]H NMR spectra of product **3e.**

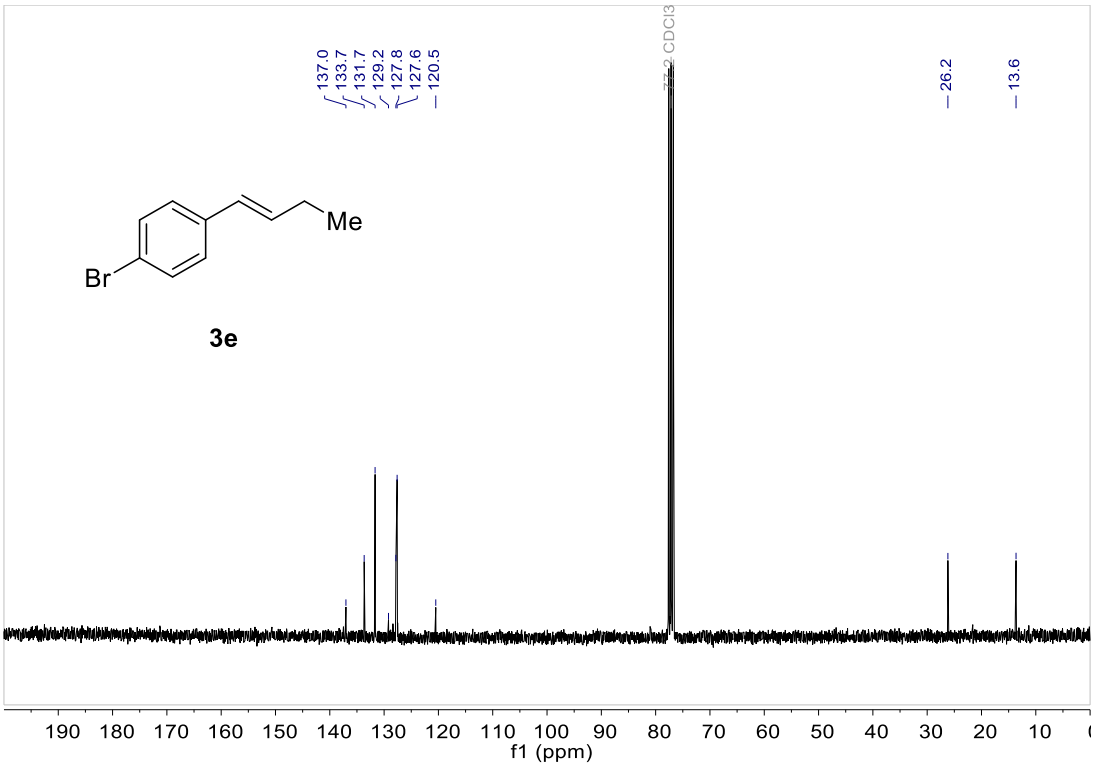

Figure S29. [13]C NMR spectra of product **3e.**

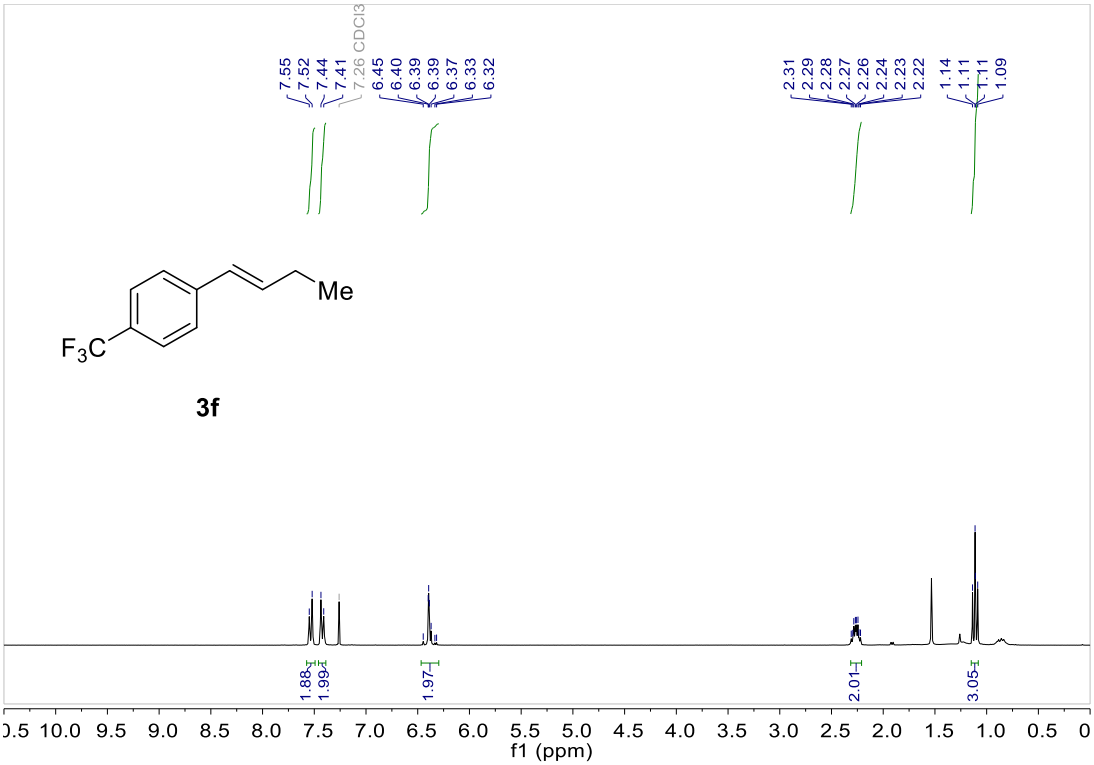

Figure S30. [1]H NMR spectra of product **3f.**

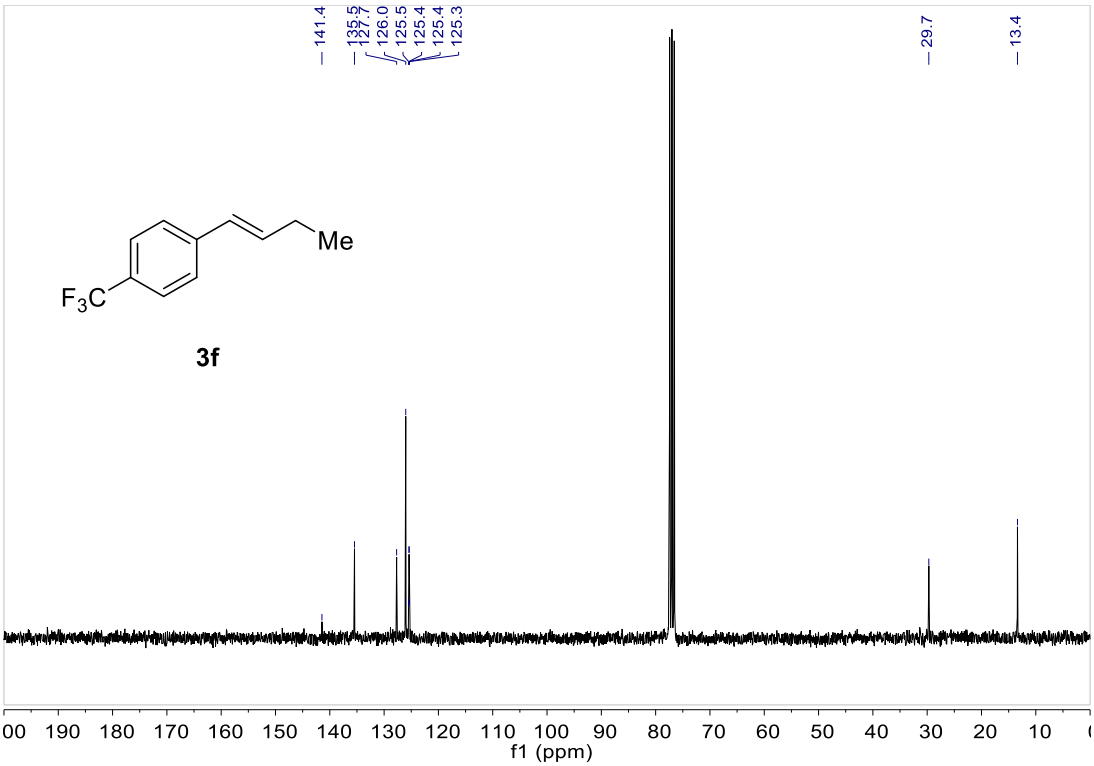

Figure S31. [13]C NMR spectra of product **3f.**

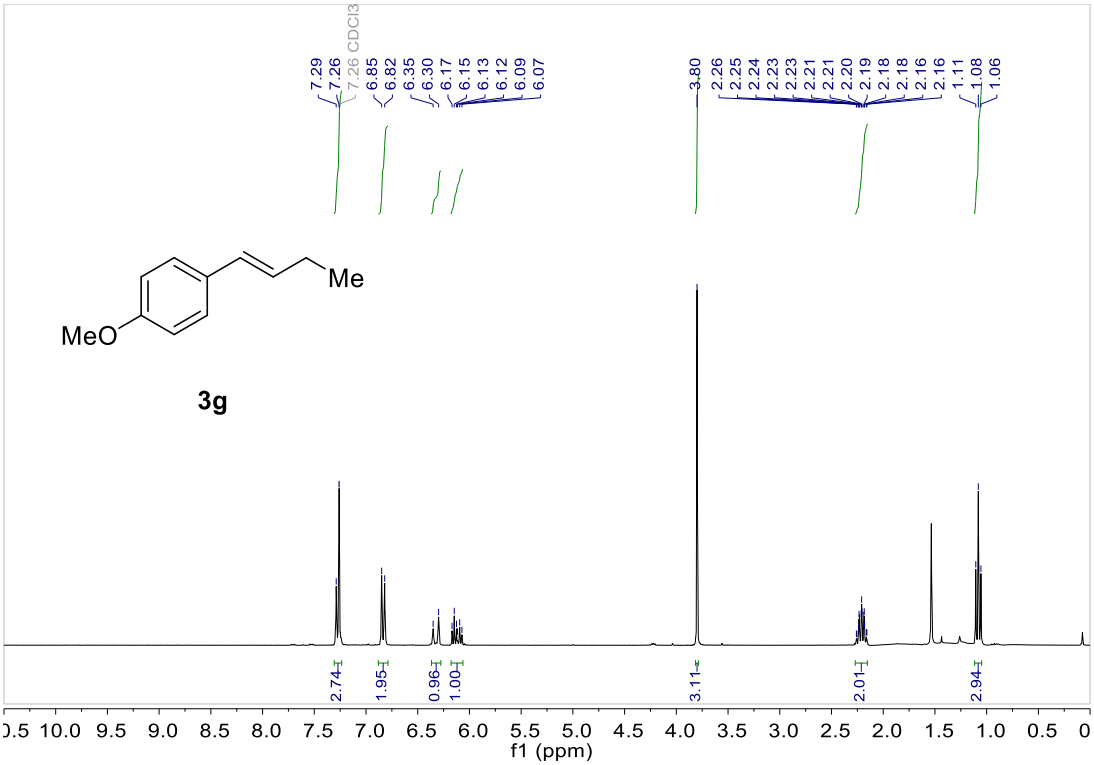

Figure S32. [1]H NMR spectra of product **3g.**

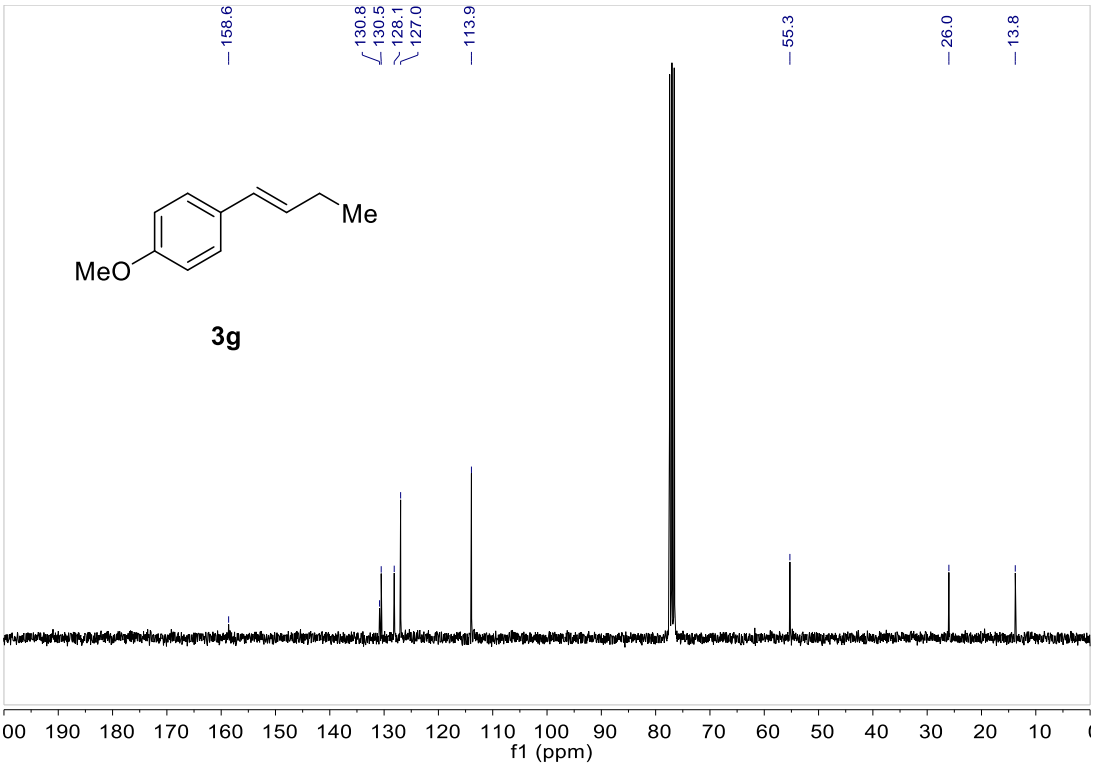

Figure S33. [13]C NMR spectra of product **3g.**

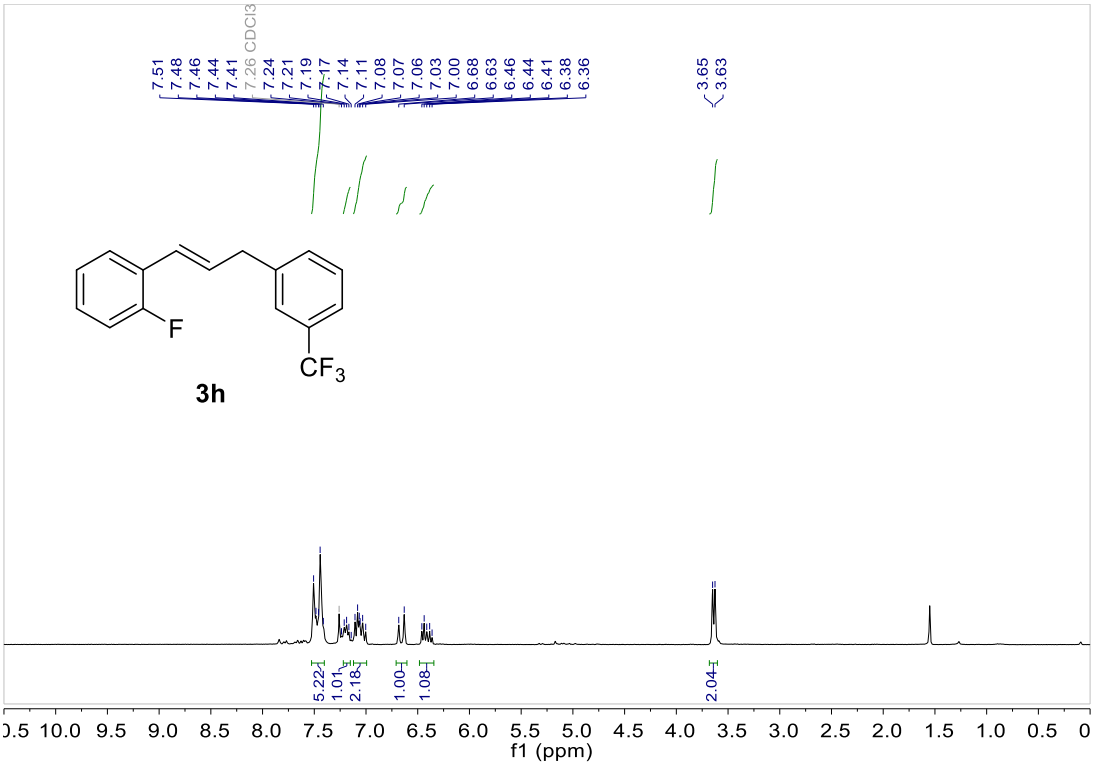

Figure S34. [1]H NMR spectra of product **3h.**

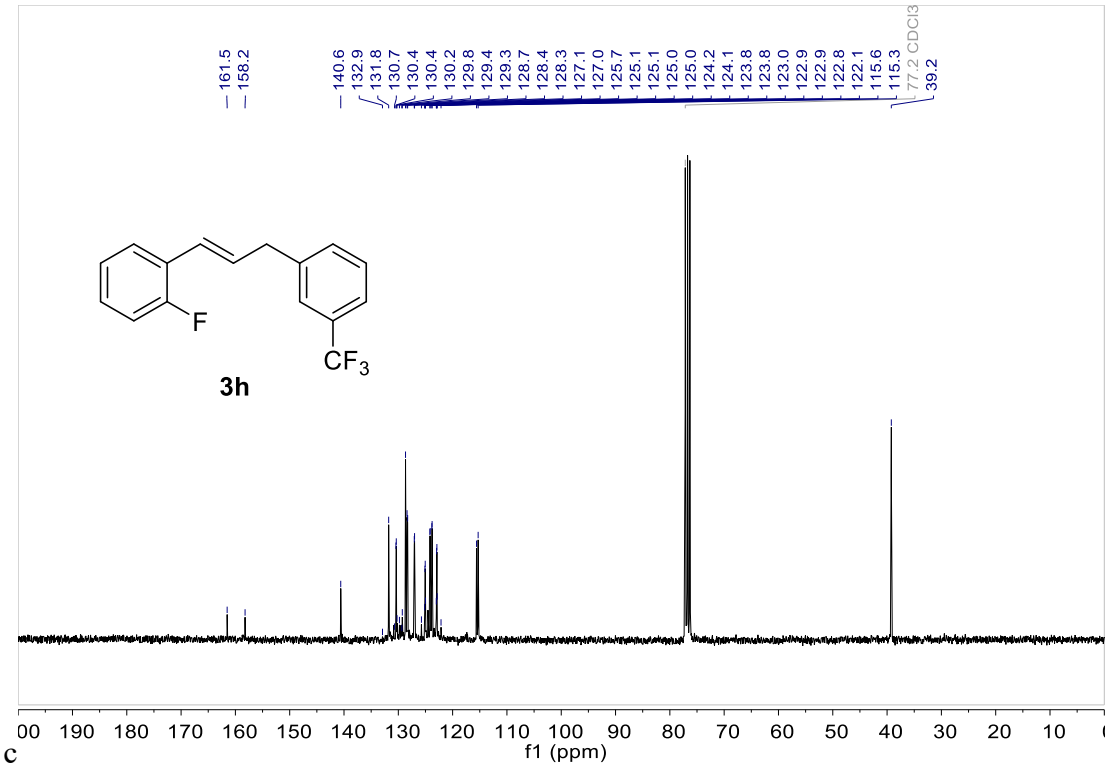

Figure S35. [13]C NMR spectra of product **3h.**

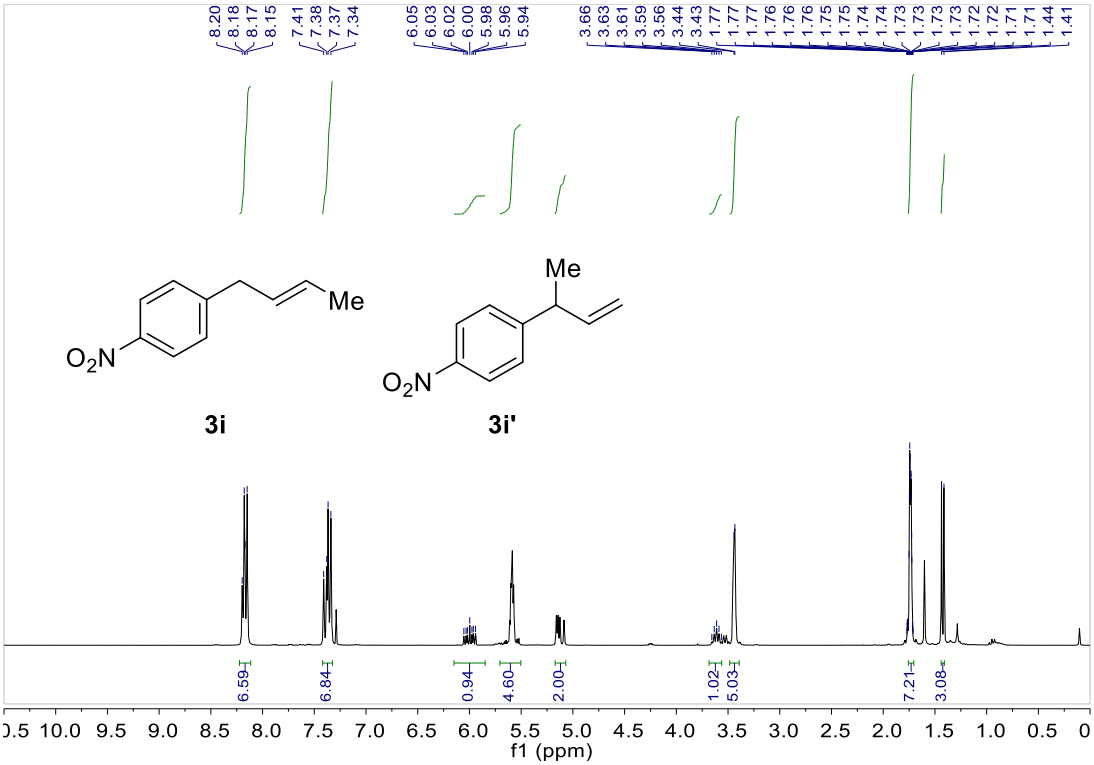

Figure S36. [1]H NMR spectra of products **3i** and **3i'.**

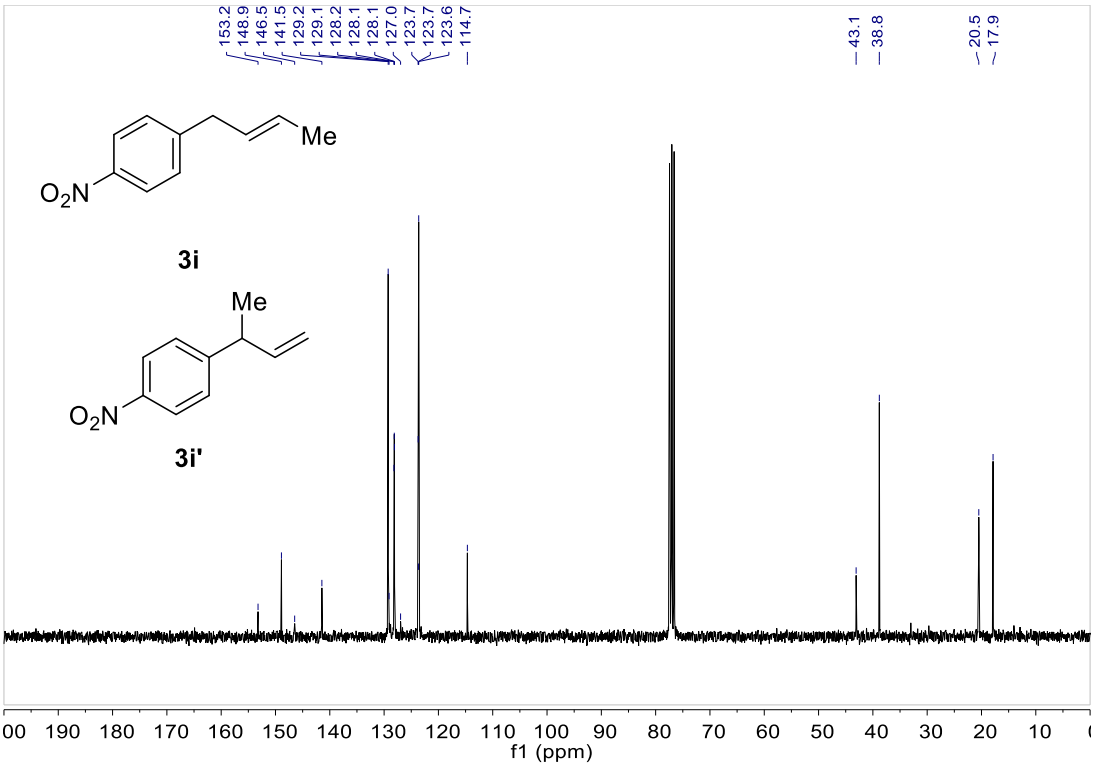

Figure S37. [13]C NMR spectra of products **3i** and **3i'.**

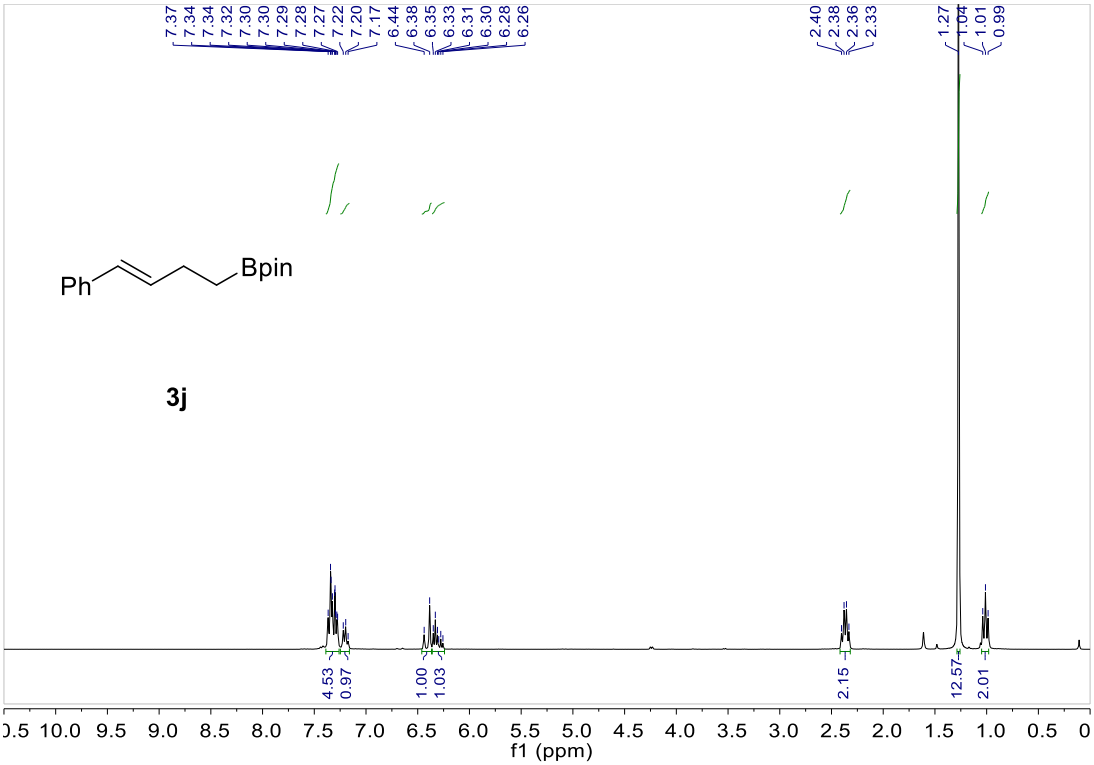

Figure S38. [1]H NMR spectra of product **3j.**

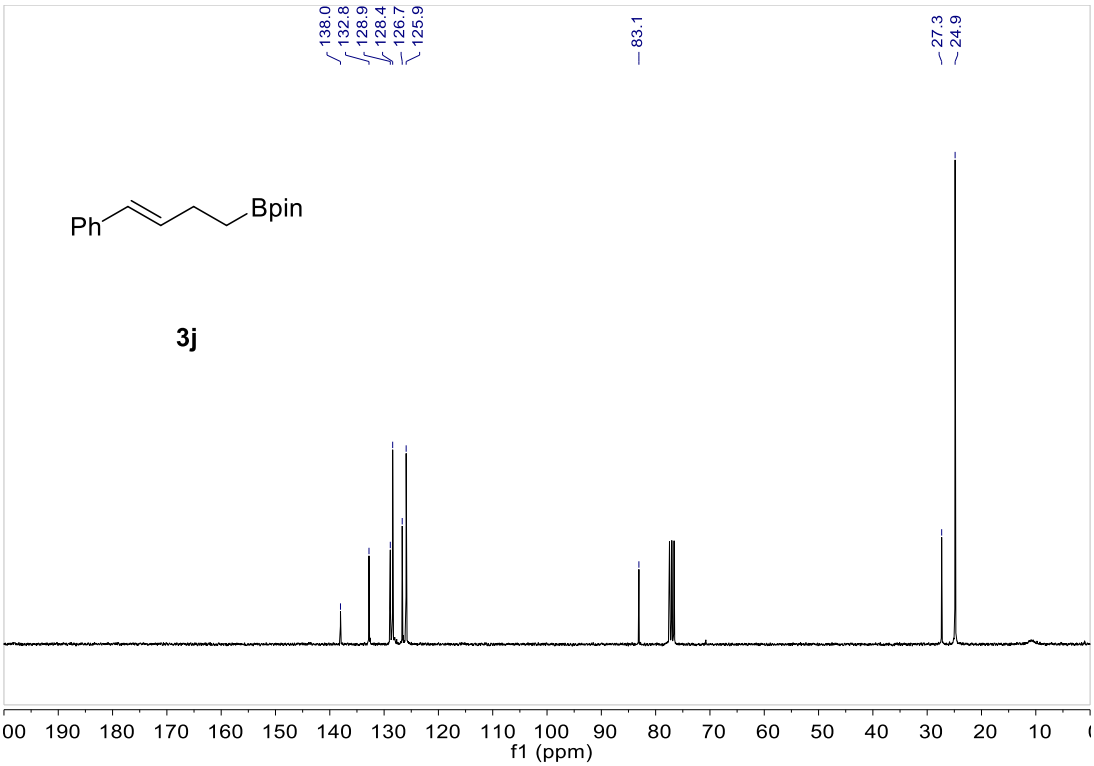

Figure S39. [13]C NMR spectra of product **3j.**

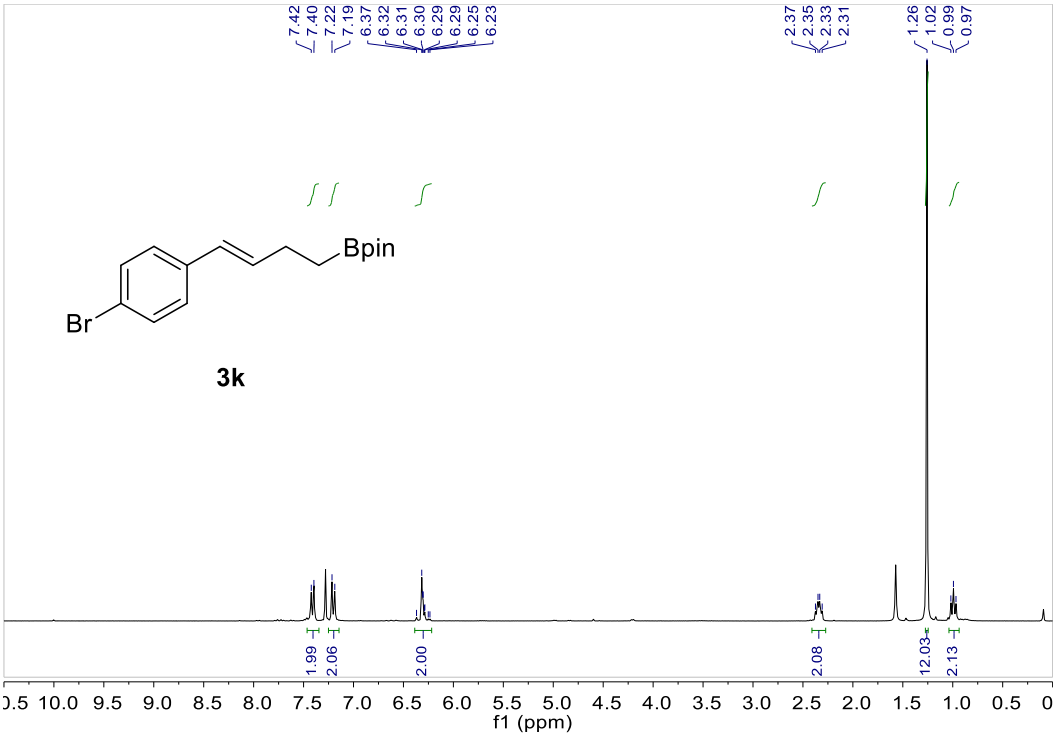

Figure S40. [1]H NMR spectra of product **3k.**

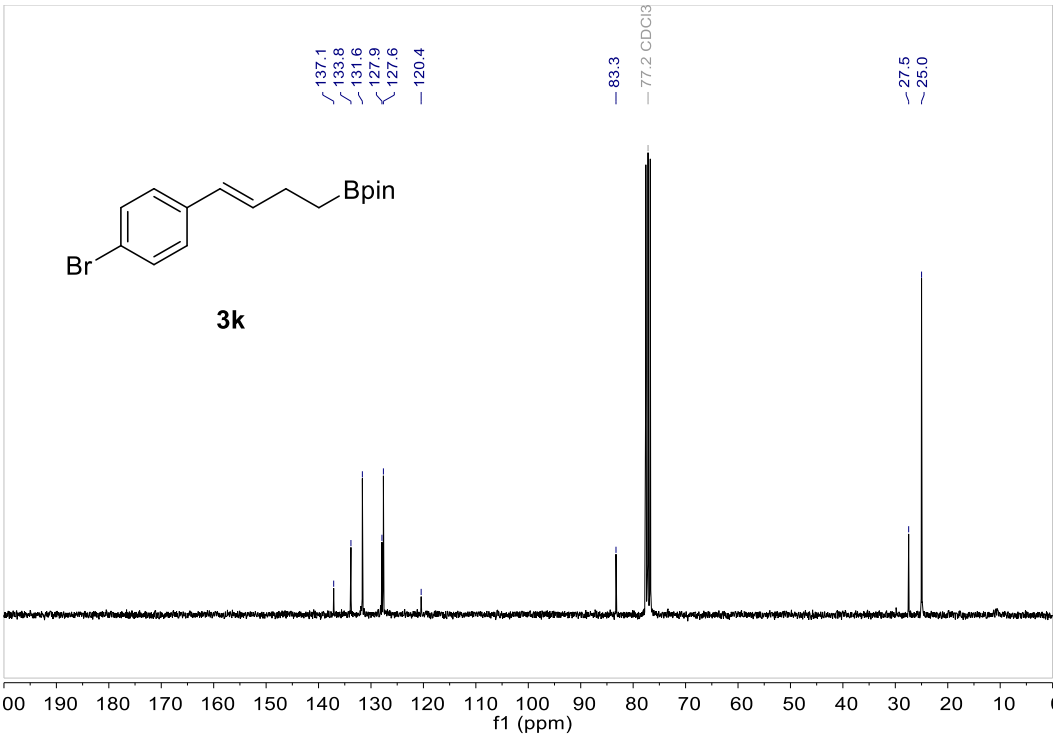

Figure S41. [13]C NMR spectra of product **3k**

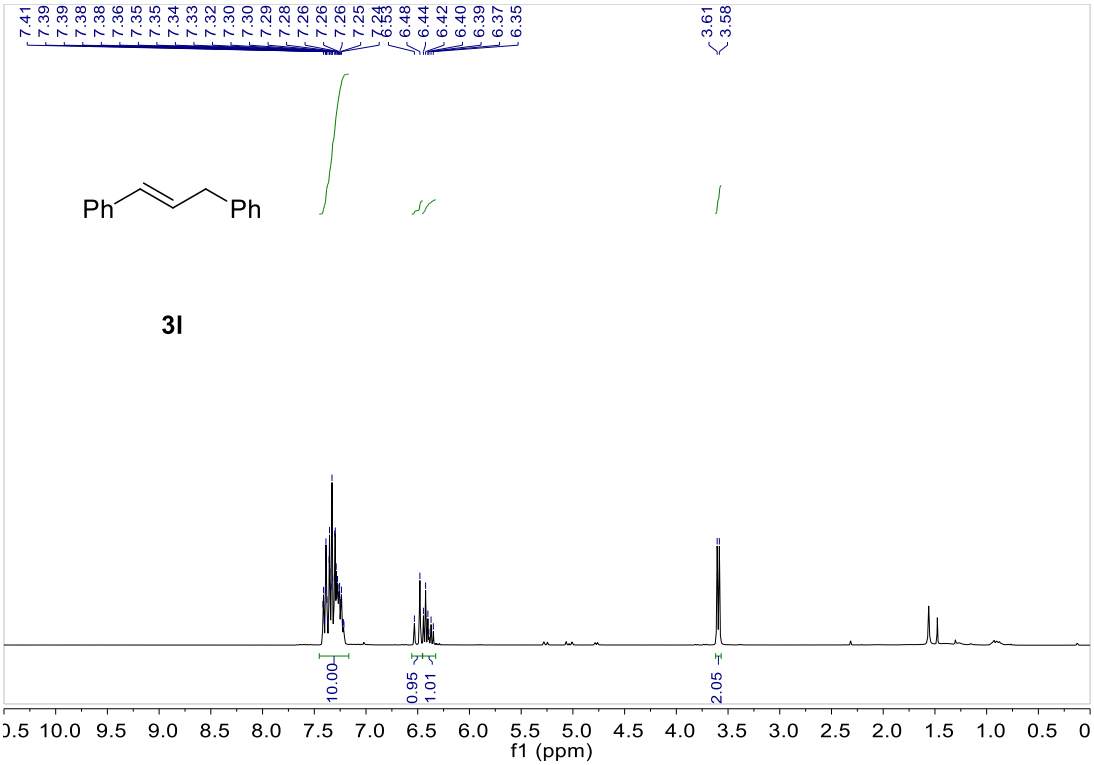

Figure S42. [1]H NMR spectra of product **3l.**

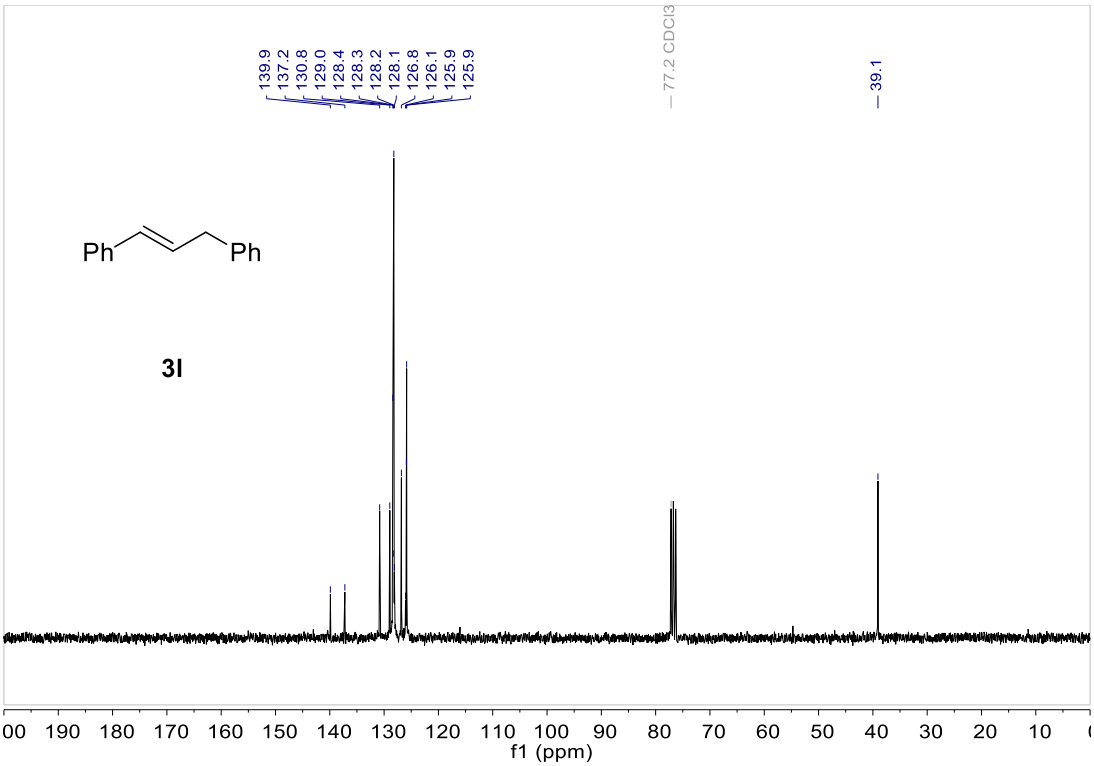

Figure S43. [13]C NMR spectra of product **3l.**

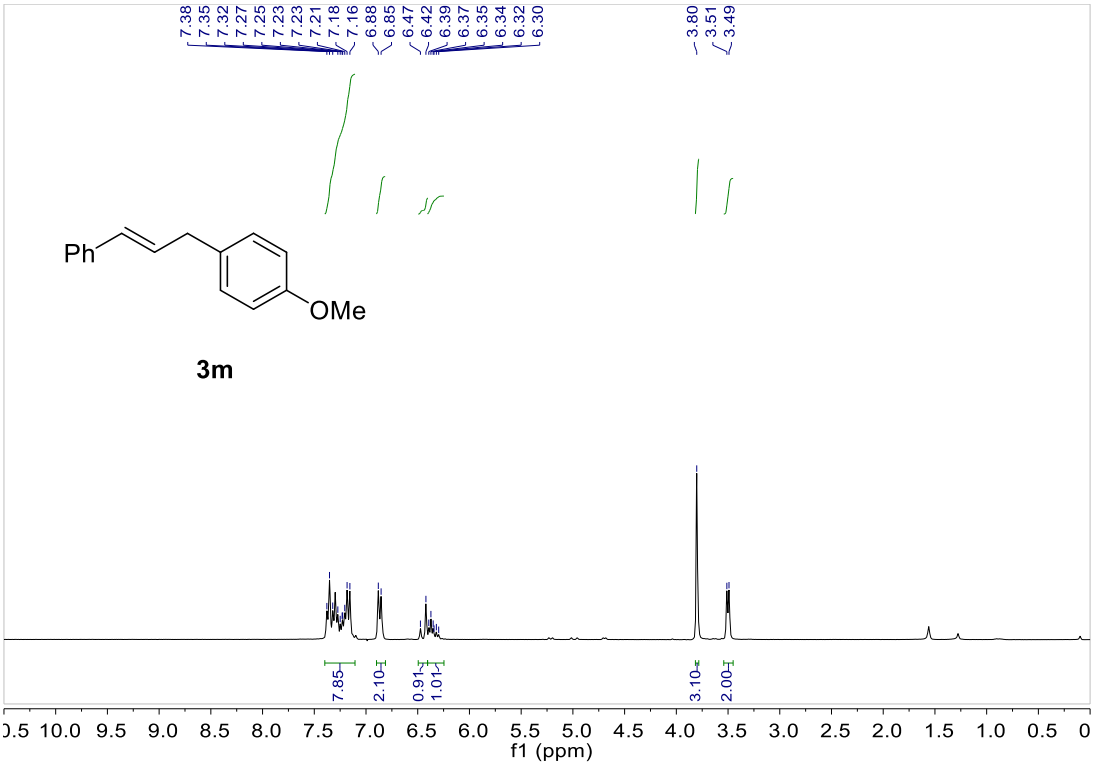

Figure S44. [1]H NMR spectra of product **3m.**

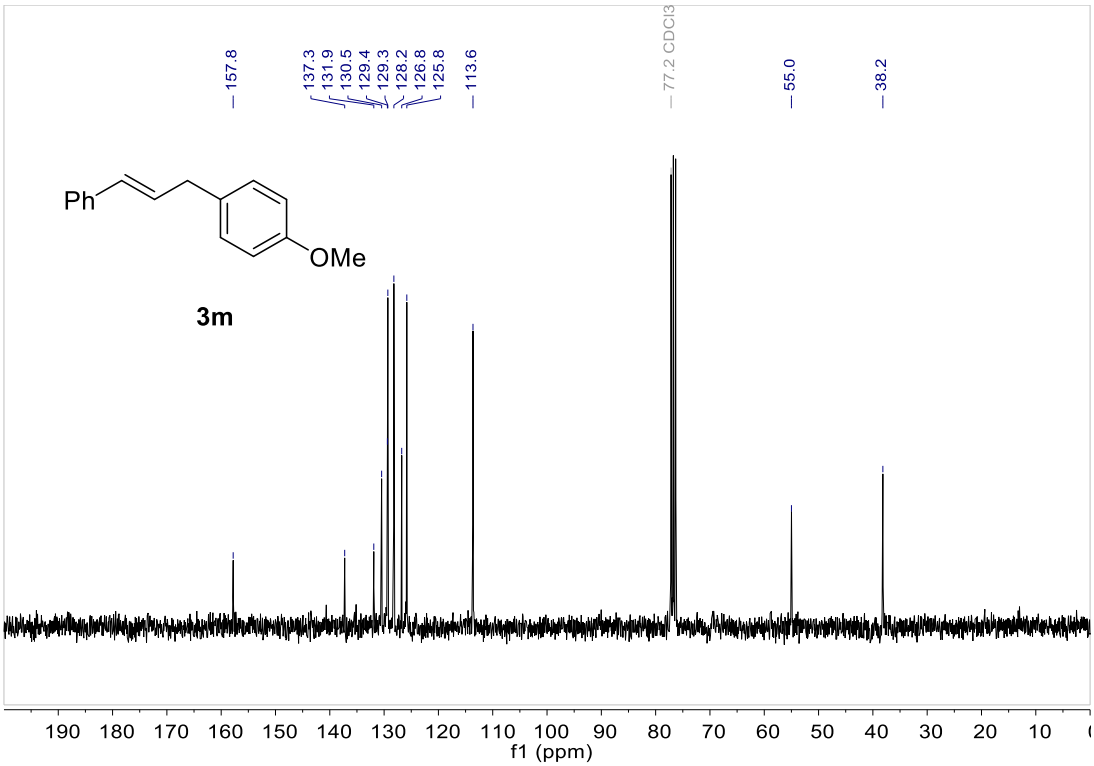

Figure S45. [13]C NMR spectra of product **3m.**

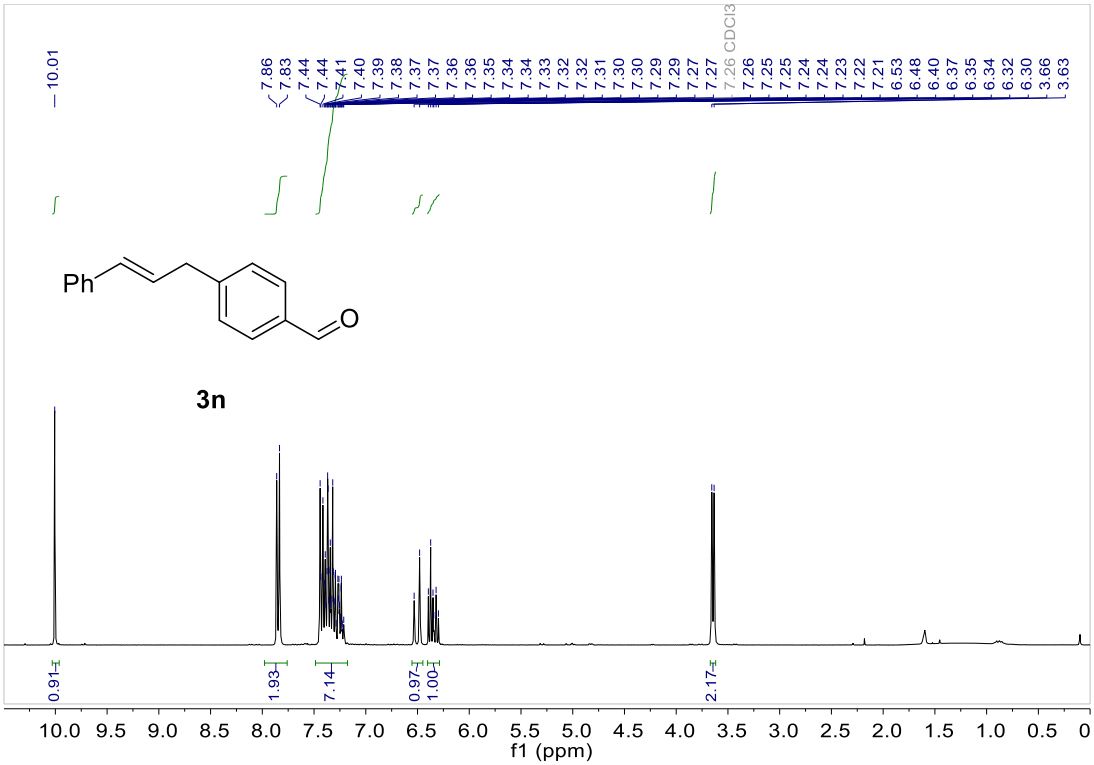

Figure S46. ^{1}H NMR spectra of product **3n.**

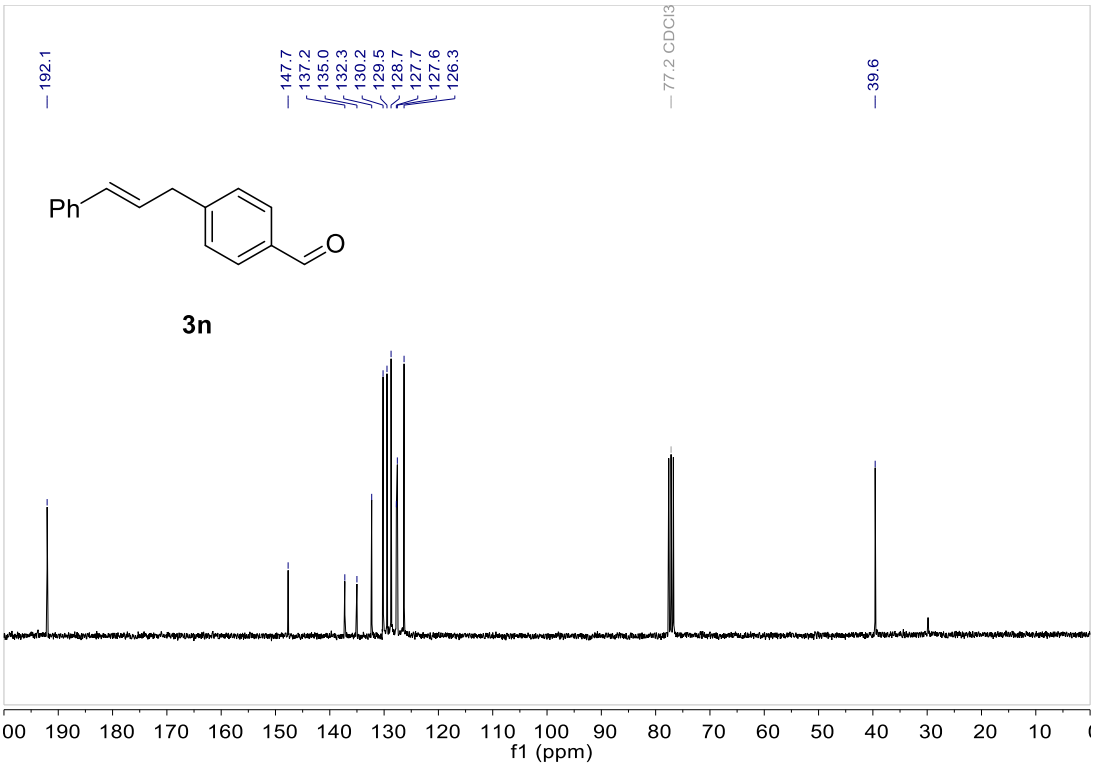

Figure S47. ^{13}C NMR spectra of product **3n.**

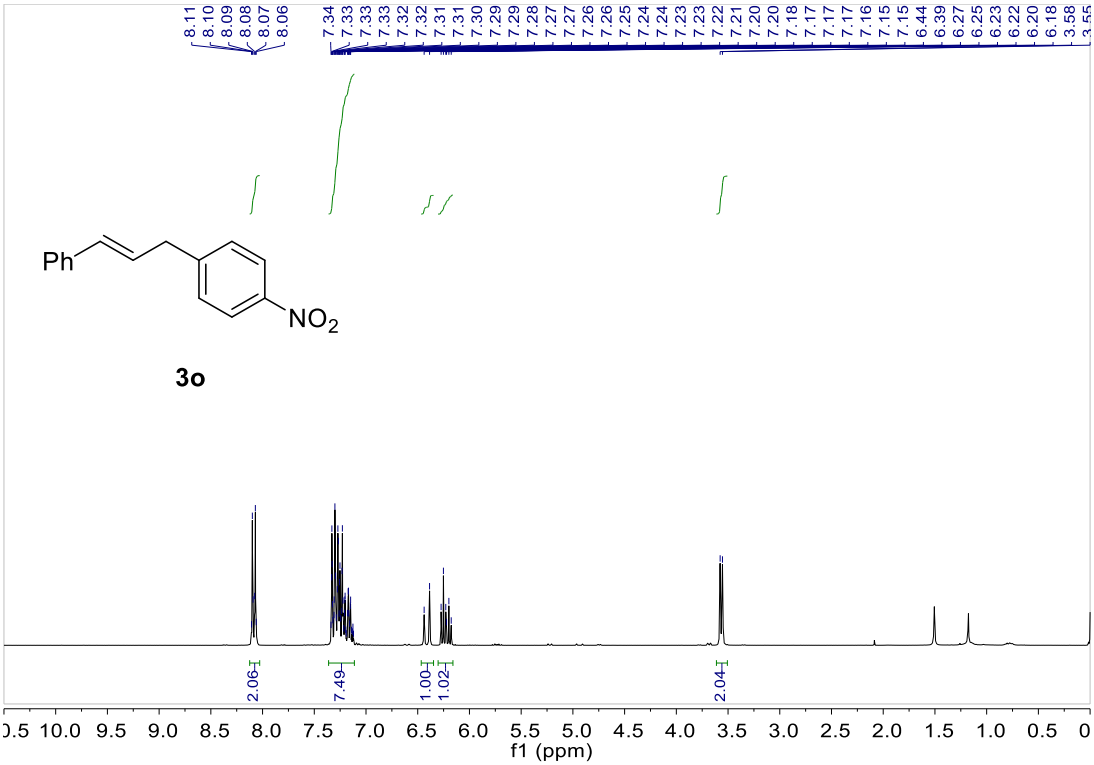

Figure S48. ^{1}H NMR spectra of product **3o.**

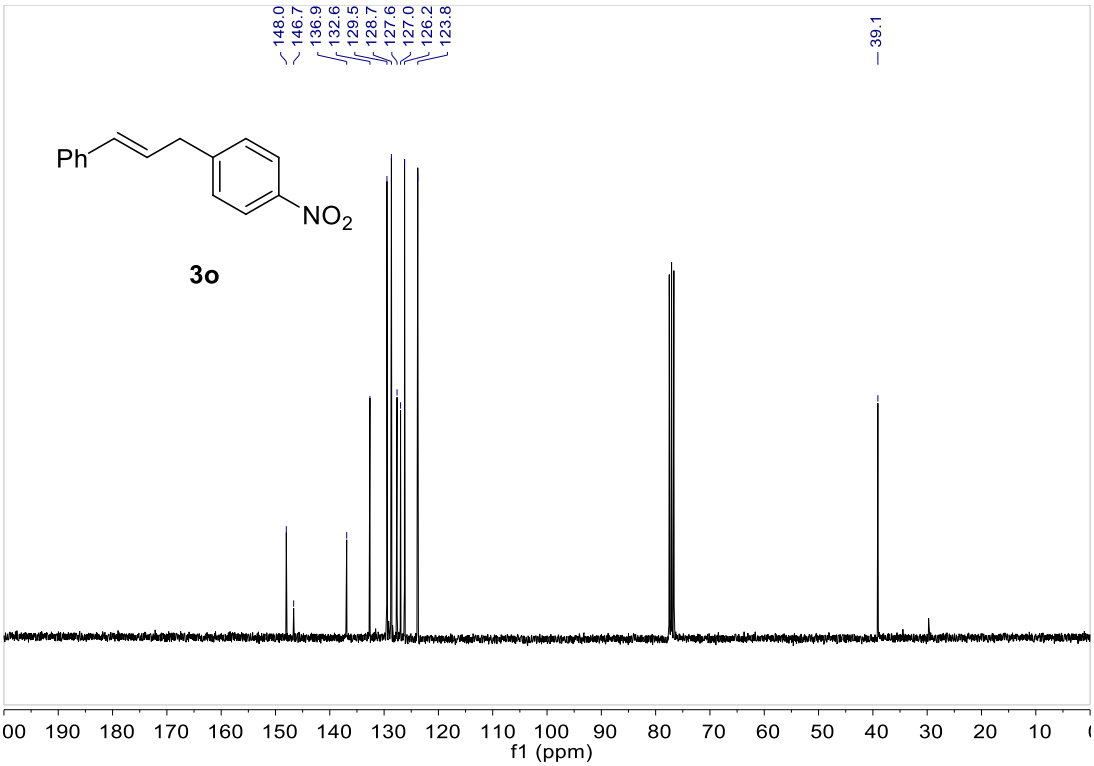

Figure S49. ^{13}C NMR spectra of product **3o.**

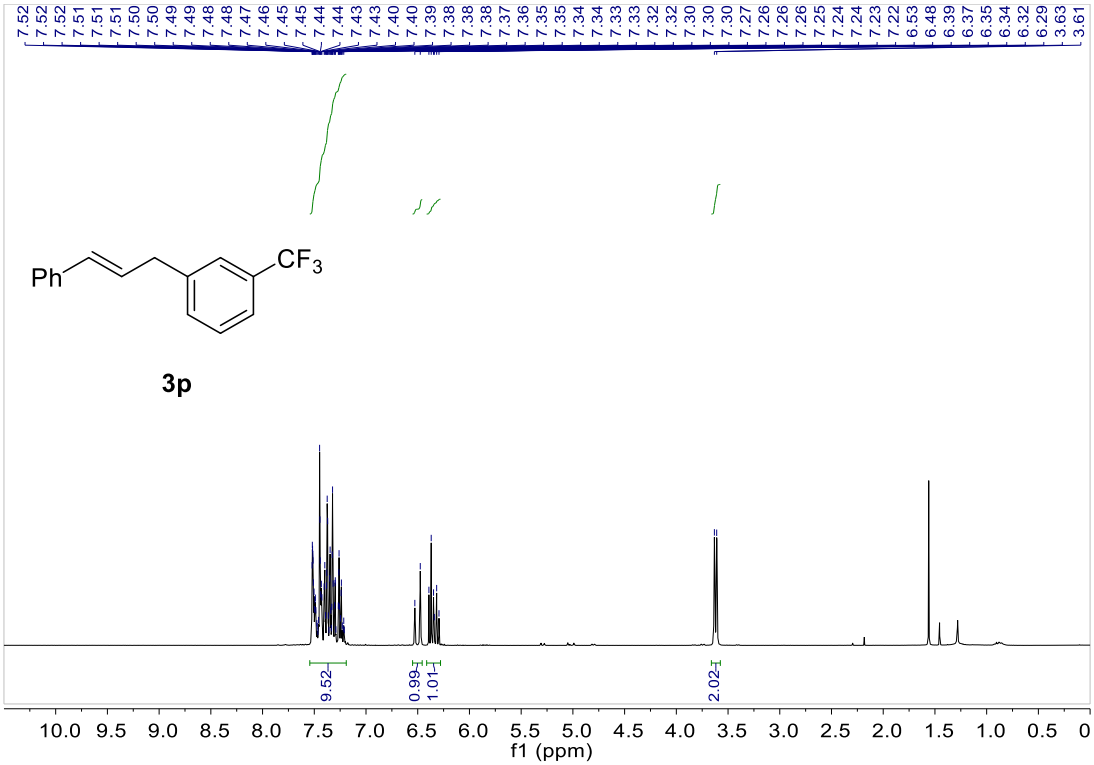

Figure S50. [1]H NMR spectra of product **3p.**

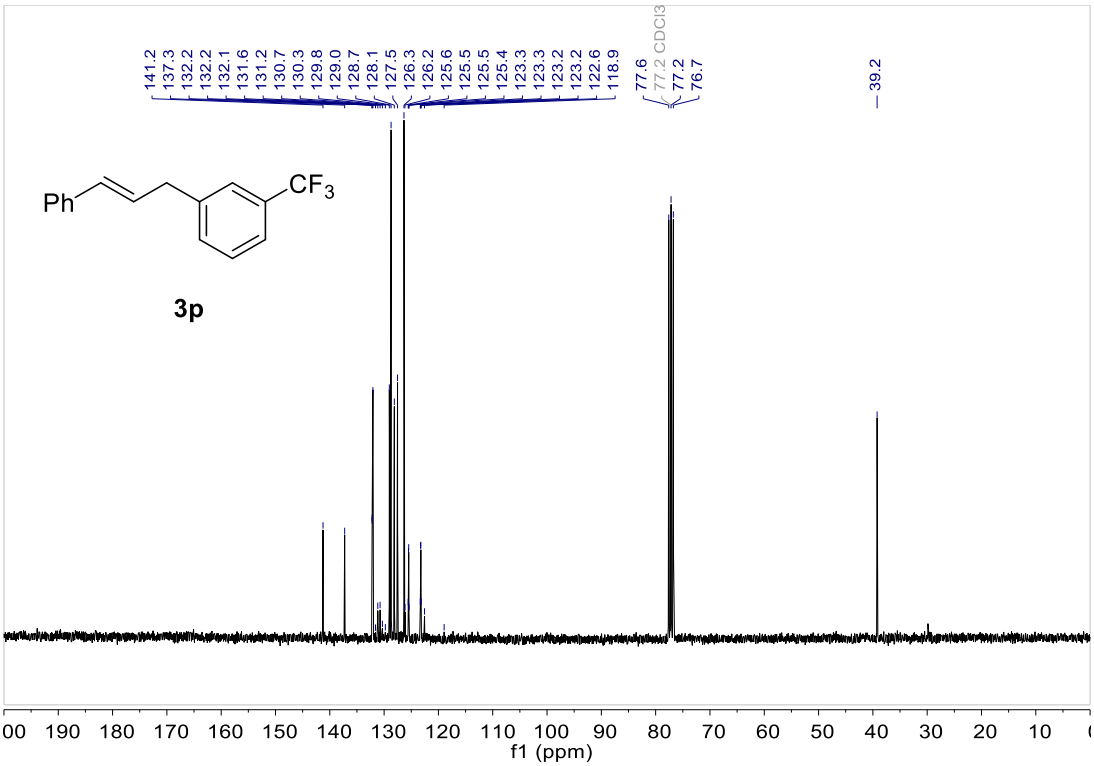

Figure S51. [13]C NMR spectra of product **3p.**

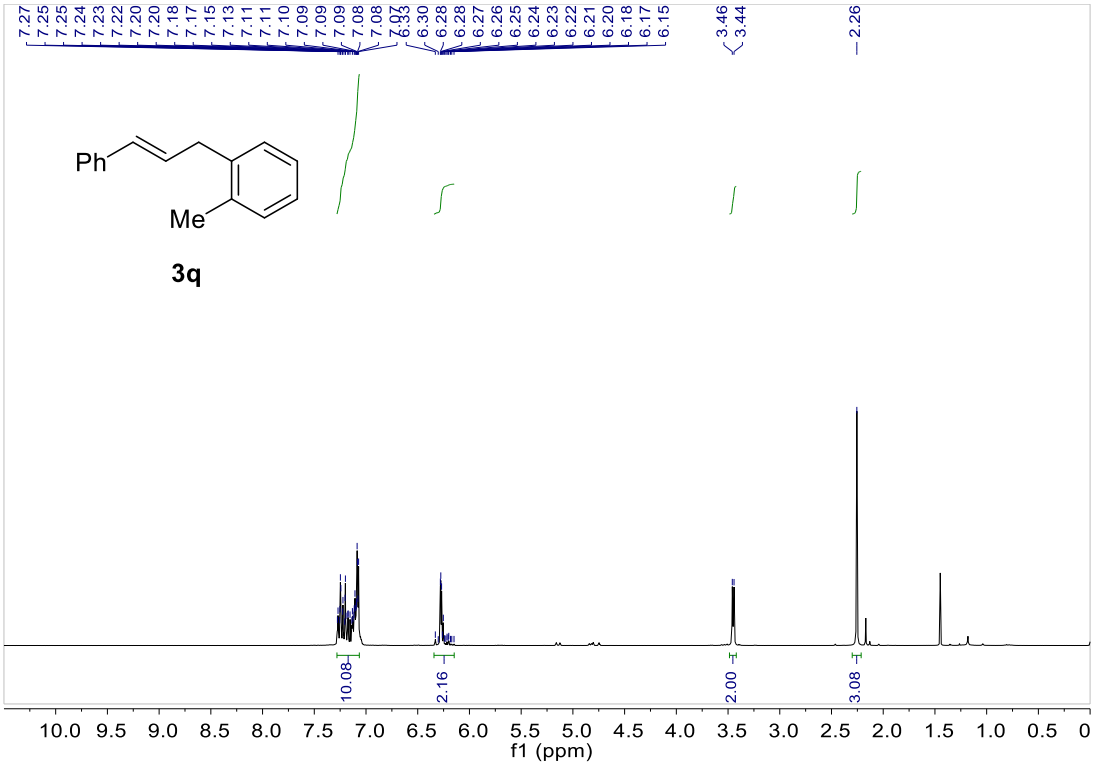

Figure S52. [1]H NMR spectra of product **3q.**

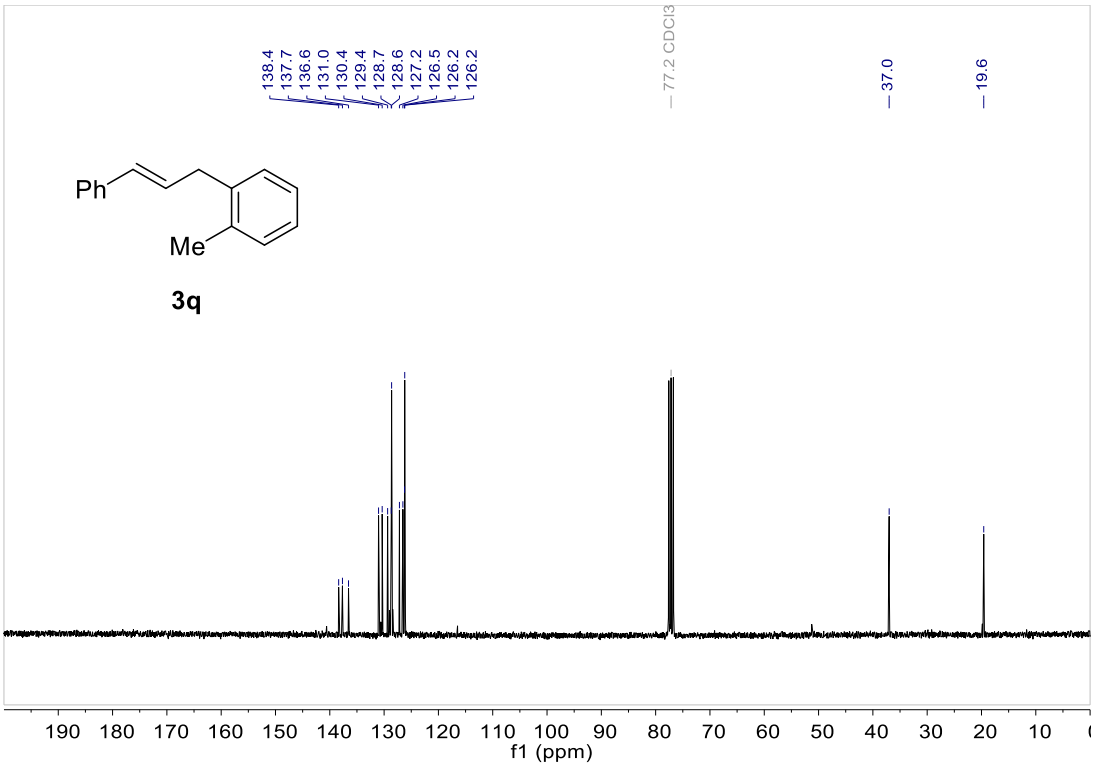

Figure S53. [13]C NMR spectra of product **3q.**

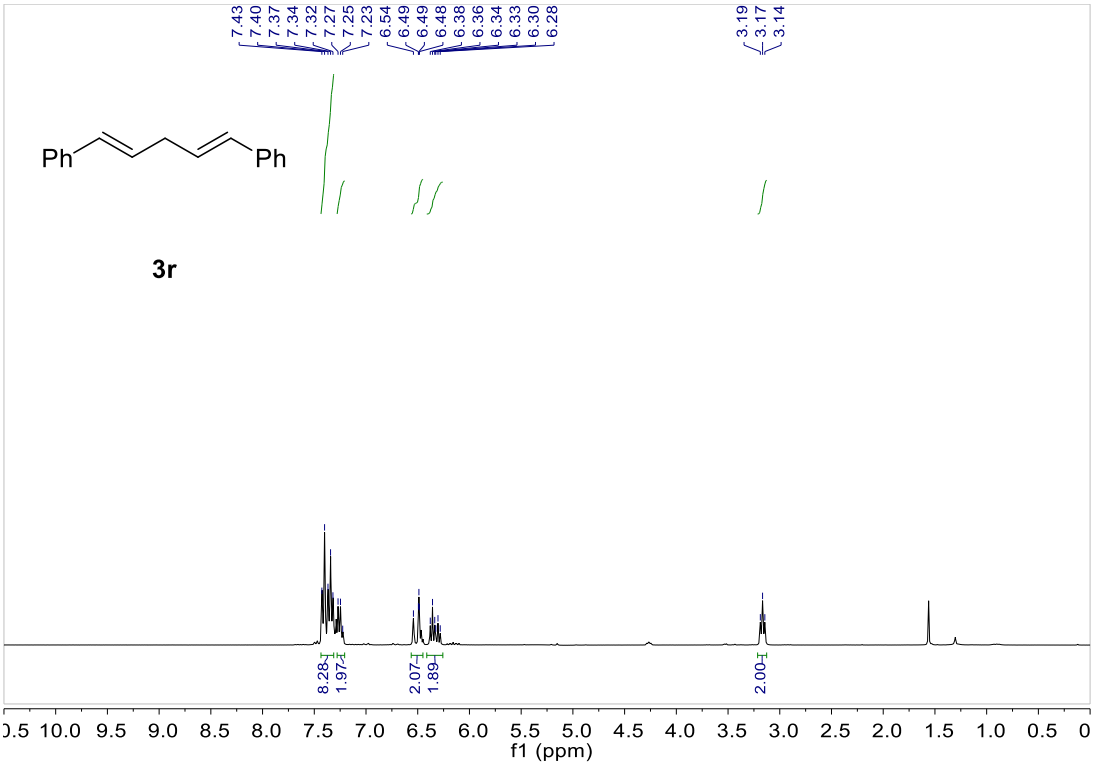

Figure S54. [1]H NMR spectra of product **3r.**

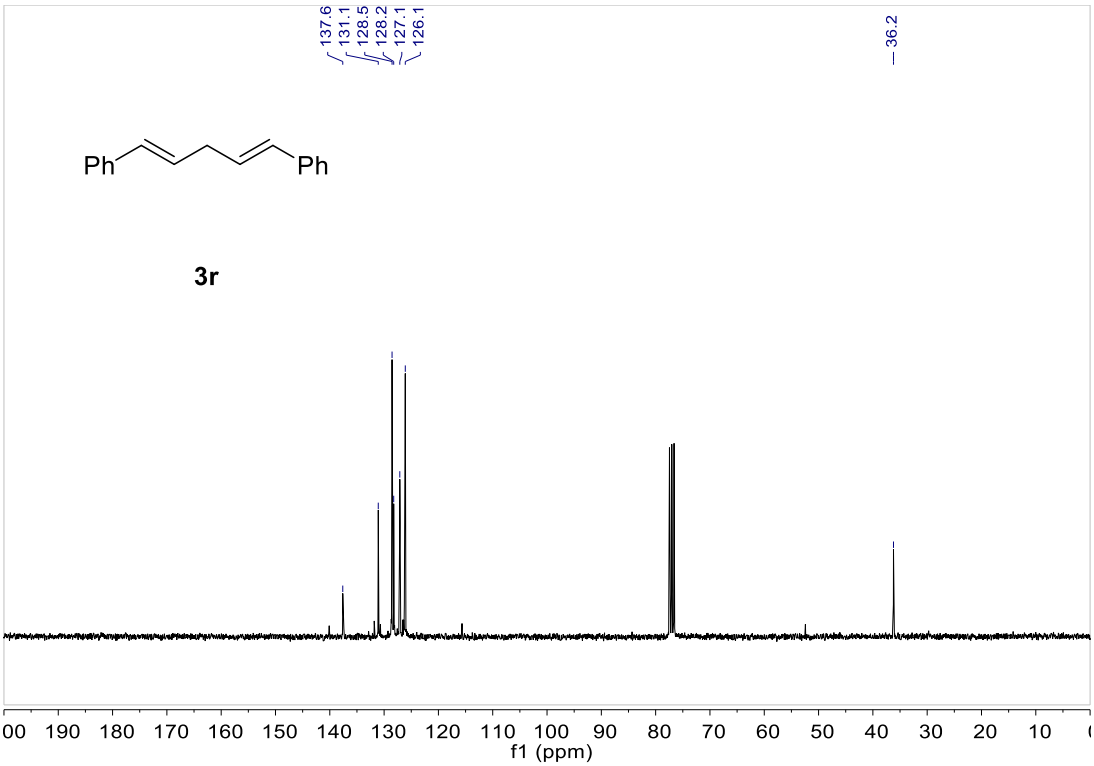

Figure S55. [13]C NMR spectra of product **3r.**

7. Stability after catalysis

After its use in the catalytic reactions, several studies were done to confirm the stability of **MUV-22**, including XRPD (to check the crystallinity), XPS (to check the oxidation state of the Pd centres), SEM (to examine the morphology of the crystals), TEM (to discard the formation of Pd nanoparticles), EDAX (to check the Pd, Fe and Cl content), and gas sorption (to check the porosity). The solid was recovered by decantation from the reaction crude and the excess of Cs_2CO_3 and KF was disolved with a buffer solution of AcOH/NaOAc (pH= 4). The solid was then recovered by decantation, washed and decanted three times with MeOH and dried overnight under vacuum, resulting in **MUV-22-PC** (post-catalysis).

7.1. X-ray powder diffraction

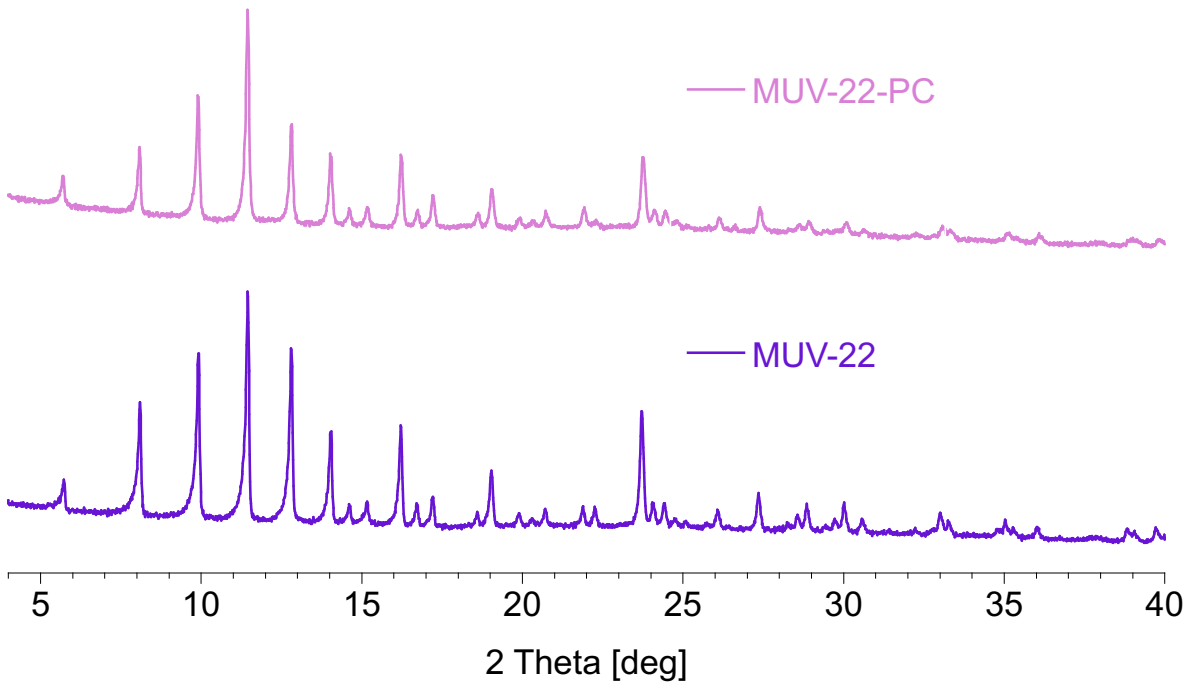

Figure S56. XRPD of **MUV-22-PC** (post catalysis) compared with as synthetized **MUV-22**.

7.2. X-ray photoelectron spectroscopy

X-ray photoelectron spectroscopy (XPS) has been performed to gain a detailed insight about possible changes in the valence state and chemical composition of **MUV-22** after catalysis. Two peaks corresponding to Pd(II) are observed, as before the catalysis (Figure S57), with complete absence of any Pd(0), thus discarding the possible formation of Pd nanoparticles. Furthermore, the full spectrum of **MUV-22-PC** (shown in Figure S58) shows the exchange between the chloride ligands by fluoride ligands that was produced upon its use as a catalyst.

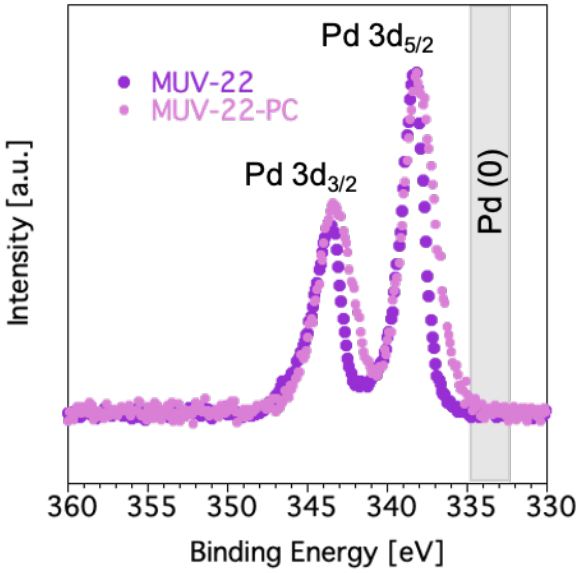

Figure S57. XPS of **MUV-22** before catalysis (dark purple) and post-catalysis (light purple).

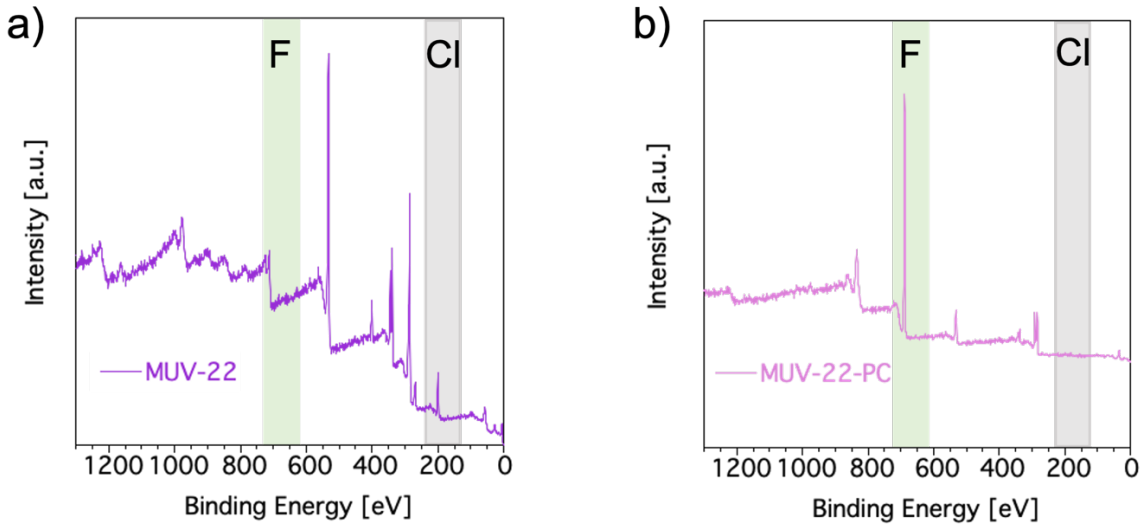

Figure S58. Full spectrum of XPS of **MUV-22** before catalysis (a) and post-catalysis (b), showing the exchange between chlorine and fluorine atoms.

7.3. EDAX

EDS analysis has been performed to gain detail of the quantities of Fe:Pd:Cl at the surface of **MUV-22** after catalysis. The ratio betwen Pd and Fe is maintained to 1.0:2.0. However, the peak corresponding to Cl disappears, with appearance of an additional peak corresponding to F, in agreement with XPS results (Figure S58).

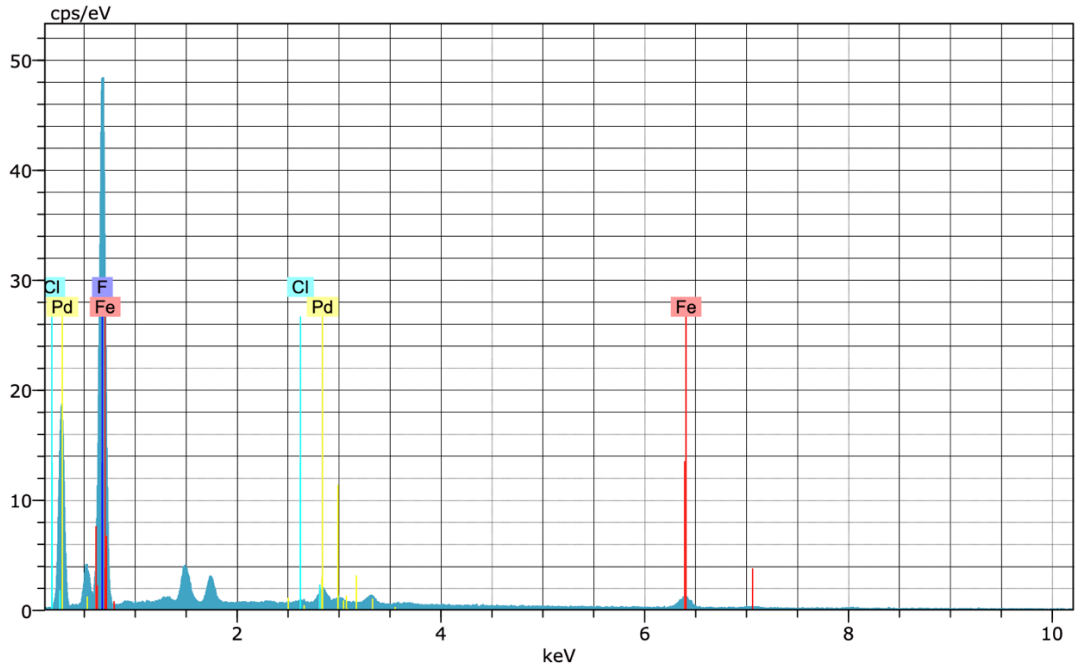

Figure S59. EDS after the catalysis of **MUV-22** showing fluorine exchange with chlorine. The Pd:Fe ratio remains as 1.0:2.0. The blue line indicates the region where the peak corresponding to Cl should be observed.

7.4. SEM

The particle morphology and crystal size of **MUV-22-PC** is observed through SEM (Figure S60).

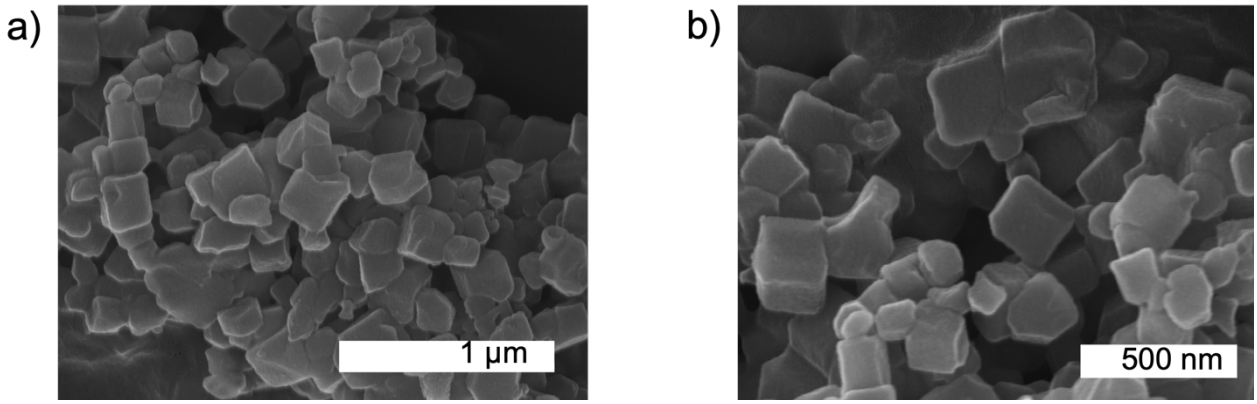

Figure S60. SEM images of **MUV-22-PC** at different scale bars: a) 1 µm; b) 500 nm.

7.5. TEM

The particle morphology and crystal size of **MUV-22-PC** were also analyzed by TEM to discard the formation of Pd nanoparticles (Figure S61). The crystal size is similar to as-synthetised **MUV-22**.

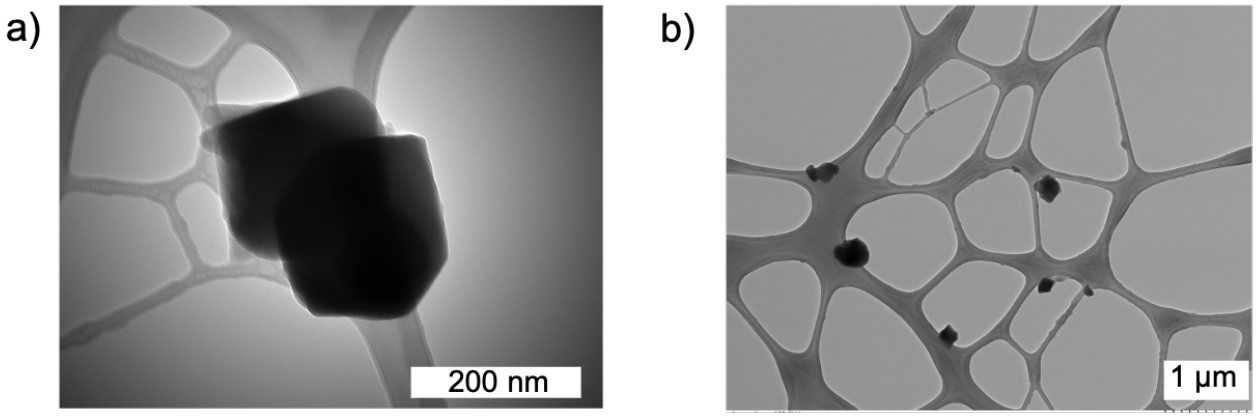

Figure S61. TEM images of **MUV-22-PC** at different scale bars: a) 200 nm; b) 1 µm.

7.6. Gas sorption

Low-pressure single-gas nitrogen adsorption isotherms were measured with the **MUV-22** recovered after catalysis (**MUV-22-PC**). The activation procedure was similar than the as-synthetized **MUV-22**. The porous nature of **MUV-22-PC** is clearly observed, although a slightly lower sorption capacity was observed. This could be due to the very small amount of **MUV-22-PC** that was used for this measurement (3.1 mg).

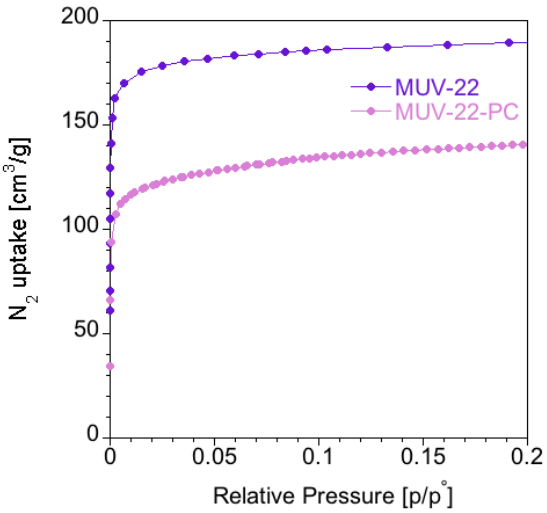

Figure S62. N_2 gas adsorption isotherms of **MUV-22** post catalysis and as-synthetized.

7.7. Inductively Coupled Plasma Mass Spectrometry (ICP-MS)

The crude of the catalytic reaction was filtered and the solution was analyzed by ICP-MS. The palladium content of the solution was determined to be 219±4 $\mu g \cdot L^{-1}$, which corresponds to 0.04% of the starting palladium, thus revealing the absence of any decomposition of the MOF during the catalysis.

8. Exchange test with KF

An experiment mixing **MUV-22** with KF in toluene at 90 ºC was performed to evaluate the influence of the catalytic mechanism in the exchange between chlorine and fluorine. As the EDS analysis shows in Figure S63, no exchange between chlorine and fluorine was observed. Thus, it can be concluded that the exchange of Cl by F occurs during the catalytic reaction.

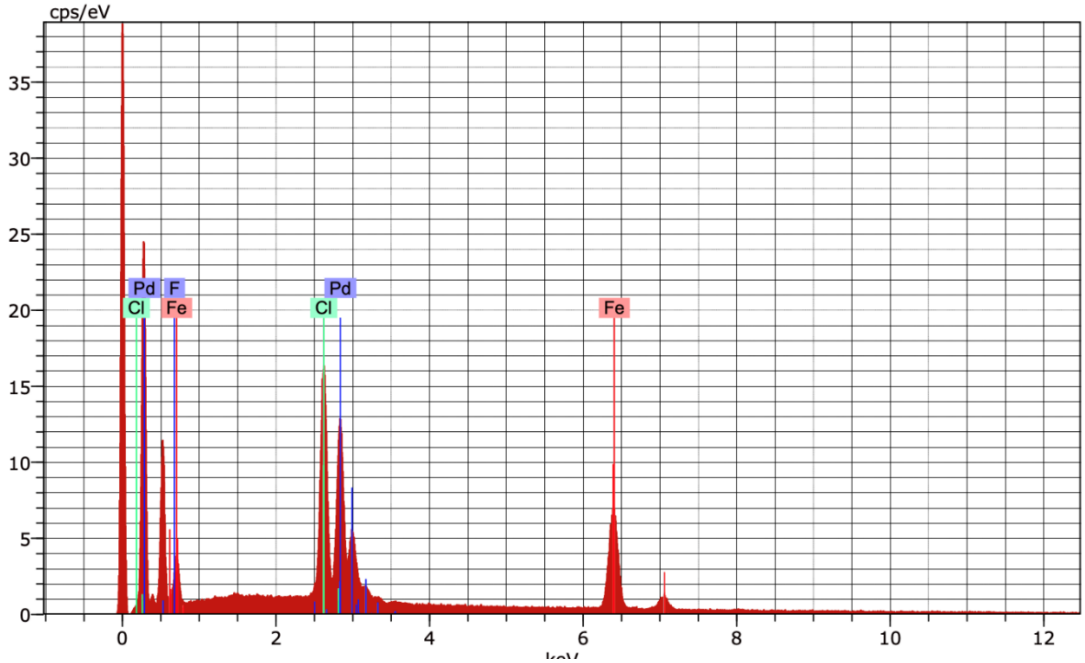

Figure S63. EDS analysis of mixing **MUV-22** with KF in toluene at 90 °C showing not fluorine exchange with chlorine. Elements with the ratio of 1.1:1.8:2.2 for Pd:Cl:Fe.

9. References

[1] Z. Q. Qin, M. C. Jennings, R. J. Puddephatt, K. W. Muir, *CrystEngComm* **2000**, *2*, 73–76.

[2] a) G. M. Sheldrick, *Acta Crystallogr. Sect. C Struct. Chem.* **2015**, *71*, 3–8. b) O. V. Dolomanov, L. J. Bourhis, R. J. Gildea, J. A. K. Howard, H. Puschmann, H. *J. Appl. Crystallogr*. **2009**, *42*, 339–341.

[3] M. K. Johnson, D. B. Powell, R. D. Cannon, *Spectrochimica Acta Part A: Molec. Spect.* **1981**, *37*, 995–1006.

[4] B. M. Choudary, K. R. Kumar, Z. Jamil, G. Thyagarajan, *J. Chem. Soc., Chem. Commun.* **1985,** 931–932.

[5] I. Bratsos, C. Tampaxis, I. Spanopoulos, N. Demitri, G. Charalambopoulou, D. Vourloumis, T. A. Steriotis, P. N. Trikalitis, *Inorg. Chem*., **2018**, *57*, 7244–7251.

[6] J.-E. Lee, J. Kwon and J. Yun, *Chem. Commun*., 2008, 733-734.

[7] W. Yang, C. Chen and K. S. Chan, *Dalton Trans*., 2018, **47**, 12879-12883.

[8] Q. Lin, B. Hu, X. Xu, S. Dong, X. Liu and X. Feng, *Chem. Sci*., 2020, **11**, 3068-3073.

[9] X. Liu, S. Liu, Q. Wang, G. Zhou, L. Yao, Q. Ouyang, R. Jiang, Y. Lan and W. Chen, *Org. Lett*., 2020, **22**, 3149-3154.

[10] S. Guduguntla, V. Hornillos, R. Tessier, M. Fañanas-Mastral and B. L. Feringa, *Org. Lett*., 2016, **18**, 252-255.

[11] J. He, Z. Jia, H. Tan, X. Luo, D.Qiu, J. Shi, H. Xu, and Y. Li, *Angew. Chem. Int. Ed*., 2019, **58**, 18513-18518.

[12] S. Gao and M. Niggemann, *Adv. Synth. Catal*., 2019, **361**, 1549-1553.

[13] E. A. Hill and M. R. Engel, *J. Org. Chem.,* 1971, **36**, 1356-1360.

[14] R. Kumar, A. Sharma, N. Sharma, V. Kumar and A. K. Sinha, *Eur. J. Org. Chem.*, 2008, **33**, 5577-5582.

[15] N. Zhu, J. Zhao and H. Bao, *Chem. Sci.*, 2017, **8**, 2081-2085.

[16] X. Yu, H. Zhao, P. Li and M. J. Koh, *J. Am. Chem. Soc.*, 2020, **142**, 18223-18230.

[17] R. K. Zhang, K. Chen, X. Huang, L. Wohlschlager, H. Renata and F. H. Arnold, *Nature*, 2019, **565**, 67-72.

[18] Y. Yasunori, T. Shingo and M. Norio, *Chem. Lett*., 2006, **35**, 704-705.

[19] K. Endo, T. Ohkubo, T. Ishioka and T. Shibata, *J. Org. Chem*., 2012, **77**, 4826-4831.

[20] Z.-Q. Zhang, B. Zhang, X. Lu, J.-H. Liu, X.-Y. Lu, B. Xiao and Y. Fu, *Org. Lett.*, 2016, **18**, 952-955.

[21] Y. Wang, Z. Shao, K. Zhang and Q. Liu, *Angew. Chem. Int. Ed*., 2018, **57**, 15143-15147.

[22] B. Yang and Z.-X. Wang, *J. Org. Chem*., 2017, **82**, 4542-4549.

[23] H. Tsukamoto, T. Uchiyama, T. Suzuki and Y. Kondo, *Org. Biomol. Chem*., 2008, **6**, 3005-3013.

[24] Y. Lee, S. Shabbir, S. Lee, H. Ahn and H. Rhee, *Green Chem*., 2015, **17**, 3579-3583.

[25] J. Qiu and R. Zhang, *Org. Biomol. Chem*., 2013, **11**, 6008-6012.

[26] B. H. Lipshutz, S. Ghorai, A. R. Abela, R. Moser, T. Nishikata, C. Duplais, A. Krasovskiy, R. D. Gaston and R. C. Gadwood, *J. Org. Chem*., 2011, **76**, 4379-4391.

[27] E. Alacid and C. Nájera, *J. Org. Chem*., 2009, **74**, 2321-2327.